


國立交通大學
光電工程研究所
碩士論文

光脈衝整形器應用於兆赫輻射波形整合之研究



**The Application of Pulse Shaping in THz
Waveform Synthesis**

研究生：吳宗翰

指導教授：潘犀靈教授

中華民國九十四年七月

光脈衝整形器應用
於兆赫輻射波形整合之研究

**The Application of Pulse Shaping in THz
Waveform Synthesis**

研究生：吳宗翰

Student: Tzung-Han Wu

指導老師：潘犀靈 教授

Advisor: Prof. Ci-Ling Pan

國立交通大學



A Thesis

Submitted to Department of Photonics &
Institute of Electro-Optical Engineering
College of Electrical Engineering
National Chiao Tung University
In partial Fulfillment of the Requirements
for the Degree of
Master of Engineering
In
Electro-Optical Engineering

July 2005

Hsinchu, Taiwan, Republic of China

中華民國九十四年七月

光脈衝整形器應用 於兆赫輻射波形整合之研究

研究生：吳宗翰

指導教授：潘犀靈教授

國立交通大學光電研究所

摘要

本論文主要是研究光脈衝整合器及其在兆赫輻射波形整合和飽和布拉格反射鏡特性之應用，在光脈衝整合器上，我們用 Gerchberg-Saxton 演算法，來設計飛秒脈衝波形。然後使用 Freezing 演算法來達成最短脈衝 (transform-limited pulse)。使用此兩種演算法來達到脈衝整合的目的，然後利用整合出的脈衝波形來合成兆赫輻射波型，用以探測兆赫輻射的基本特性。

The Application of Pulse Shaping in THz Waveform Synthesis

Student: Tzung-Han Wu Advisor: Prof. Ci-Ling Pan

Institute of Electro-Optical Engineering National Chiao Tung University

Abstract

In this thesis, it can be demonstrated that how to design and the optical synthesis technique for a desired ultrafast optical pulse with Gerchberg-Saxton (GS) algorithm. Based on the algorithm, multi-pulse with different pulse duration, two pulses with dissimilar pulse duration and single pulses with different pulse width achieved by unalike phase pattern can be accomplished. We use a new freezing phase algorithm for complete-field attributes of femtosecond ultrashort pulse with a phase-only pulse shaping apparatus. The operational principle is based on the fact that the highest peak intensity corresponds to a complete frozen-phase state of all spectral components. Femtosecond laser pulse is achieved to be the transform-limited femtosecond laser pulse by this algorithm. Pulse shaping technology has already demonstrated a strong impact as an experimental tool providing convenient control over ultrafast laser waveforms especially for THz waveform synthesis. We illustrate this technique using several experimental examples, including manipulation of the bandwidth and the pulse number of ultrafast terahertz waveforms as well as generation of different terahertz spectrum.

國立交通大學

論文口試委員會審定書

本校光電工程研究所碩士班 吳宗翰 君

所提論文 光脈衝整形器應用於兆赫輻射波形合成

合於碩士資格標準、業經本委員會評審認可。

口試委員：賴暎杰 趙如蘋
賴暎杰 教授 趙如蘋 教授

洪勝富
洪勝富 教授

指導教授：潘犀靈
潘犀靈 教授

所長：賴暎杰 教授
賴暎杰 教授

系主任：潘犀靈 教授
潘犀靈 教授

中華民國 94 年 7 月 25 日

誌謝

永遠忘不了這一段旅程，六年來的風城生涯告一段落，接踵而來的是未知的挑戰與充滿期待的未來。

六個春去秋來的日子裡要感謝的人很多，首先我要特別感謝我的指導教授潘犀靈博士給我的指導與鼓勵，提供良好的學習環境跟研究資源，在研究上及待人處世的態度方面也讓我受益良多。而在研究實驗的過程當中，很感謝學長李兆達博士的細心指導讓我在遇到實驗困境時能夠順利突破，且有所啟發，接下來感謝師大謝美莉教授在實驗校正方面給於無私的幫助以致我們實驗可以順利進行。其次我要感謝我的研究伙伴，澎湖仔，在這五百多各日子裡所一起串起的回憶將會化成我對你的祝福，祝福你順利完成夢想，也別忘了生命的邀約，『即使我在這多霧的轉角稍稍遲疑也沒什麼好擔心的，就等這霧散盡之後，我就啟程』。接著我要感謝老劉，學姐 Moya, Mika, 小高, 小壯, CC, 小冷, 學妹這兩年來所帶來的歡樂跟喜悅。而隊長，羅誠，阿隆，家任，最後因為有你們的陪伴，往後人生將有所不同。

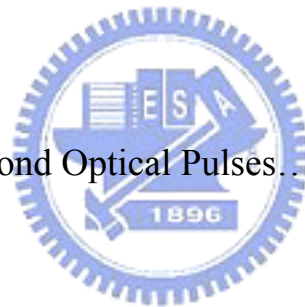
家人，有你們的支持跟鼓勵，讓我有勇氣去追求自己的人生。老姐，二姐謝謝你們在我困苦無助時讓我傾吐苦水，並給予我精神上的支持，更感謝郁歆這一年來的互相扶持，也因為這樣更讓我們堅定要去完成夢想，不再遲疑！老爸，老媽你們辛苦了，三言兩語不能道盡我對你們的感謝跟思念，因為有你們的愛才能讓我無後顧之憂的沈浸在學習的喜悅當中，今天的成就都要歸功於你們。

所有的結局都已寫好，對於未來也將悄悄啟程。

2005 7 至夏風城

Contents

1. Introduction.....	1
2. All- reflective Pulse Shaping Apparatus.....	3
2-1.Principles of Pulse Shaper	3
2-2.Schematic and Real Setup of Our Phase-only Pulse Shaper.....	5
2-3.The Calibration of Spatial Light Modulator (SLM) System.....	7
3. Synthesis of Femtosecond Optical Pulses.....	14
3-1.Mode-locked Ti: sapphire Laser.....	15
3-2.Adaptive Pulse Shaping with Freezing Phase Scheme.....	16
3-3.Synthesis of Femtosecond Optical Pulses with Gerchberg-Saton Algorithm.....	22
4. The Application of Pulse Shaping in THz Waveform Synthesis.....	32
4-1.Principles of Optically Excited and Detected THz Radiation and	



its Applications.....	35
4-2.Simulation of THz Radiation with Drude-Lorentz Model.....	38
4-3. Generation of THz Radiation Using Chirp Controller of Femtosecond Optical Pulses	43
4-4. Generation of THz Radiation Using Multi-Peak Femtosecond Pulses.....	49
5. Conclusion and Future Prospect.....	54
6. References.....	56



LIST of FIGURES

2-1 Pulse shaping by linear filtering. (a) Time-domain view. (b) Frequency domain view.....	5
2-2. The schematic and real setup of our phase-only pulse shaper.....	7
2-3. The transfer ratio related between level and intensity of laser intensity.....	8
2-4. Typical modulation transfers function for an SLM with NM wavelength range...8	
2-5. The database curve that is the relation between the phase and the level.....	9
2-6. The result of interference. The optical distant in the one laser beam of half spot size in interferometer optical path is altered by increase voltage of SLM, and the pixels of SLM increased voltage have different optical distant from that no voltage increased. The Figs show the phenomenon which the voltage is raised from 970 to 1480 showed in figure (A) to figure (Q). The optical distant are increased gradually, the interferometric fringes are shifted. So we use the image data to calculate the relation between increased voltage of pixel and phase shifted value SLM induced.....	12
2-7 The database curve that is the relation between the phase and the level with interference method	13
3-1. Schematic of the adaptive coherent control system with an all reflective 4- <i>f</i> pulse shaper used in this study.....	19
3-2. Flow chart depicts the procedure used to implement the freezing-phase scheme into the theoretical and experimental studies.....	19

3-3. Adaptive phase added on liquid crystal spatial light modulator for various stages.....	19
3-4 Transform-limited Autocorrelation trace after freezing.....	21
3-5 Retrieved amplitude and phase of pulse, checked with typical 64x64 SHG FROG [18], after freezing.....	21
3-8 The flow chart of GS algorithm. ● Start point. ● Stop point.....	23
3-9 The spectrum of laser.....	24
3-10. (a) The GS results of simulated one pulse (pulse width is 169fs) and it's the phase.....	25
3-10. (b) The GS results of simulated two peaks pulse (pulse spacing is 836fs) and it's the phase.....	26
3-10. (c) The GS results of simulated square pulse and it's the phase.....	27
3-11. The convergent time of square pulse.....	28
3-12(a)(b)(c)(d) display the GA experimental results of autocorrelation traces which experimental spacing are 214fs (theory spacing is 201fs), 300fs (theory spacing is 290.16fs), 379.6fs (theory spacing is 379.44fs), 559.49fs (theory spacing is 513.36fs).....	29,30
3-13.(e)(f) represent the results of autocorrelation traces from GA when the target pulses are multi-pulse at different pulse spacing on the time axis: (e)eight pulses, pulse spacing 188fs, (f)ten pulses, pulse spacing 180fs.....	31
4-1. (a) Waveforms of photocurrents and (b) their time derivatives as a function of time at trapping times ζc of 0.1, 0.5, 1.0, 2.0, and 5.0 ps. The waveform of the THz pulse is similar to that of the time derivative of the photocurrent.....	42

4-2 The waveforms of the THz pulse for laser pulse widths Δt of 80, 150, and 200 fs. As shown in Fig. 2 the THz pulse widens as the excitation laser pulse width increases. The spectral bandwidth of THz radiation also changes considerably as the width of the laser pulse changes.....43

4-3 The waveforms of the THz pulse for different relaxation time t_s of 30, 33, 34, 35, 36fs. As shown in Fig. 3 the THz waveform does not change significantly with the change of the relaxation time t_s , but the amplitude is become large as the relaxation time increased.....43

4-4 The different pulse width which is broadened by negative or positive chirp is made by SLM. Red line means the pulse broadened by positive chirp and break line means the negative chirp.....45

4-5 The relation between the chirp and pulse width.....46



4-6 The setup of terahertz time domain spectroscopy and pulse shaping system.....46

4-7 shows the THz waveform generated with different pulse width we synthesize.

The THz pulse widens as the excitation laser pulse width increases, the slimily phenomenon in simulation showed in **fig4.2** is obtained. For blue curve and green curve, laser pulse width = 900fs and 600fs. Purple curve represent the THz radiation is yielded by transform-limited laser.....47

4-8 The spectrum of THz radiation generated with different pulse width we synthesize. Base on the result of experiment, the spectrum of THz radiation widens as the excitation laser pulse width decreases. For block curve and green curve, laser pulse width = 900fs and 600fs. Red curve represent the THz radiation is yielded by transform-limited laser.....48

4-9 The schematic diagram of experiment arrangement Pump laser pulses enter the apparatus and are spectrally dispersed in an optical pulse shaper which has a computer-controlled array of optical masks. The numbers of pulses in the train of optical pump pulses now generate the shaped terahertz pulses. The shape of the terahertz pulses are collected and guided by gold-coated parabolic mirrors. Femtosecond laser pulse as a probe beam with time delayed by motor stage and the shape THz pulse collinearly impinged on another dipole antenna with the GaAs substrate to detect THz radiation.....50

4-10. (a) (b) (c) Pulses trains of one, two and three pulses generate THz radiation. THz temporal shapes and the spectra of the THz pulses are shown in the left, and the right figure panel.....52

4-11 The THz spectrum is generated by increasing numbers of optical pulses and the amplitude in spectrum is enhanced in some certain frequency.....52

4-12 The THz radiation with the different number of pulse in the temporal domain.....53

Chapter1. Introduction

Femtosecond solid-state lasers bring a number of important advantages, including substantially improved output power and stability and new physical mechanism for pulse generation advantageous for extremely short pulses. Equally important, the use of solid-state gain media has also led to simple and many researchers are now setting their sights on practical and low cost ultrafast laser systems usable for real-world applications. The focus of this thesis is femtosecond pulse shaping and its application, a topic complementary to femtosecond pulse generation. Over the past decade powerful optical waveform synthesis (or pulse shaping) methods have been developed which allow generation of complicated femtosecond laser waveforms according to researcher specification. Pulse shaping technology has already demonstrated a strong impact as an experimental tool providing unprecedented control over ultrafast laser waveforms for spectroscopy, nonlinear fiber optics. Coupled with the recent advances and resulting widespread availability of femtosecond laser, as well as advances in femtosecond pulse characterization techniques, femtosecond pulse shaping is poised to impact many divers and additional application. A number of approaches for ultrafast pulse shaping including the ability to generate coherent optical pulse with arbitrary shape, precisely control frequency and phase have been advanced. Here we adopted widely and successful method in which waveform synthesis is achieved by spatial light modulation (SLM), where the SLM allows reprogrammable waveform generation under computer control. A recent review by Weiner provides a broad account of femtosecond [1-2]. Other useful reviews include Ref. [3-5].

Transform-limited process is important before shaping optical waveform, so

adaptive phase-only pulse shaping technology was adopted. We use the new phase-freezing scheme which is for characterization and adaptive control of coherent optical pulses to achieve the goal, transform-limited laser pulse. The complicated ultrafast optical waveform according to user specification was designed and synthesized by Gerchberg-Saxton algorithm [6]. This thesis presents theoretical and experimental studies on the design, characterization, and adaptive coherent control of ultrafast optical pulses. The application of the methodology on THz waveform synthesis based on radiation from ultrafast current surges in photoconductive switches excited by shaped optical pulses which was investigated by pulse shaping system are also presented[7]. Our technique provides a simple way to generate flexible terahertz waveforms, like as shaped pulse trains, broadband pulse and tunable narrow-band radiation.

This thesis is organized as follows. We describe in Section II the principle of pulse shaping, all-reflective pulse shaping apparatus and the calibration of spatial light modulator (SLM) system. Section III describes the synthesis of femtosecond optical pulses including adaptive pulse shaping with freezing phase scheme and synthesis of femtosecond optical pulses with Gerchberg-Saxton algorithm. In Section IV, pulse shaping technique was applied to THz waveform synthesis and studying of strained saturable Bragg reflector. First of all, we present terahertz radiation theory and THz radiation was simulated by Drude-Lorentz model. Second, THz waveform generated using optical pulse sequences are appeared. Section V summarizes the experimental results and future prospect. Finally, references are listed.

Chapter 2. All-reflective Pulse Shaping Apparatus

In this chapter, we shall introduce the principle of pulse shaping and our phase-only pulse shaping apparatus, how to calibrate spatial light modulator (SLM). First of all, we describe in section 2.1 femtosecond pulse shaping theory. Second, the Phase-only pulse shaping system and some critical procedures for aligning the pulse shaper will be described in Section 2.2. In section 2.3, we use two different methods which are liquid crystal and interference physics to calibrate spatial light modulator and get modulation transfer function for an SLM with infrared ray wavelength range.

2.1. Principles of Pulse Shaper



The femtosecond pulse shaping approach described in this thesis is based on the linear, time-invariant filter, a concept well known in electrical engineering. Linear filtering is commonly used to process electrical signals ranging from low frequencies (audio) to very high frequencies (microwave). Here we apply to linear filtering to generate specially shaped optical waveforms on the picosecond and femtosecond time scale. Of course, the hardware needed for programmable linear filtering of femtosecond laser pulses looks very different from the familiar resistors, capacitors, and inductors used for linear filtering of conventional electrical signals.

Linear filtering can be described in either the time domain or the frequency domain, as depicted in Fig. 2-1. [1] In the time domain, the filter is characterized by

an impulse response function $h(t)$. The output of the filter $E_{out}(t)$ in response to an input pulse $E_{in}(t)$ is given by the convolution of $E_{in}(t)$ and $h(t)$

$$E_{out}(t) = E_{in}(t) * h(t) = \int dt' E_{in}(t') h(t - t')$$

Where $*$ denotes convolution. If the input is a delta function, the output is simply $h(t)$. Therefore, for a sufficiently short input pulse, the problem of generating a specific output pulse shape is equivalent to the task of fabricating a linear filter with the desired impulse response. Note that instead of the term “impulse response function,” which is common in electrical engineering, $h(t)$ may also be called a Green function, which is a common terminology in some other fields.

In the frequency domain, the filter is characterized by its frequency response $\mathcal{H}(\omega)$. The output of the linear filter $\mathcal{E}_{out}(\omega)$ is the product of the input signal $\mathcal{E}_{in}(\omega)$ and the frequency response $\mathcal{H}(\omega)$.

$$\mathcal{E}_{out}(\omega) = \mathcal{E}_{in}(\omega) \mathcal{H}(\omega).$$

The relation between $\mathcal{H}(\omega)$ and $h(t)$, $\mathcal{E}_{out}(\omega)$ and $E_{out}(t)$, $\mathcal{E}_{in}(\omega)$ and $E_{in}(t)$ are Fourier transform pairs.

$$H(\omega) = \int dt h(t) e^{-i\omega t}$$

And

$$h(t) = \frac{1}{2\pi} \int dt H(\omega) e^{i\omega t}$$

The input spectrum $\mathcal{E}_{in}(\omega)$ is equal to unity, and the output spectrum is equal to the frequency response of the filter, for a delta function input pulse. Hence, due to the

transform relations, synthesis of a desired output waveform can be achieved by manipulation a filter with the required frequency response. Our pulse shaping approach is described most naturally by means of this frequency domain point of view.

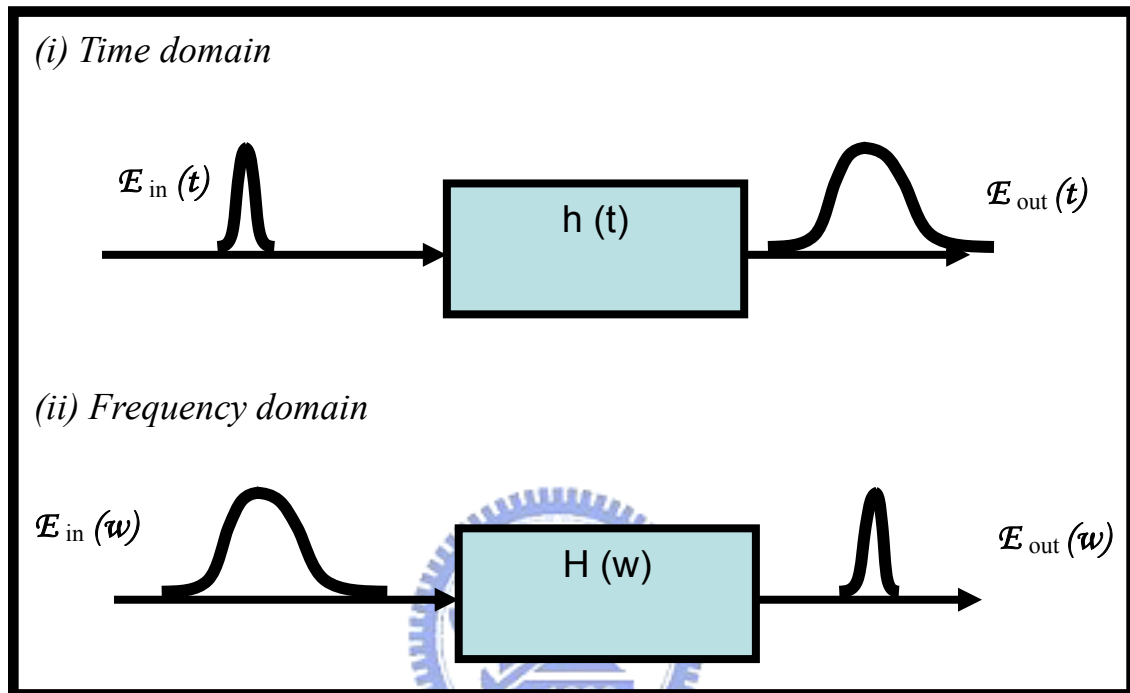
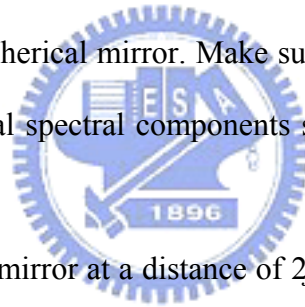


Fig. 2-1 Pulse shaping by linear filtering. (a) Time-domain view. (b) Frequency domain view.

2.2. Schematic and Real Setup of Our Phase-only Pulse Shaper

The phase –only pulse shaper system we constructed consists of a pair of gratings 600 lines/mm, two spherical reflectors with a focal length of $f = 20\text{cm}$. Optical pulses shaping is accomplished using a programmable spatial light modulator[8] (SLM Cambridge Research and Instrumentation Inc. (CRI) Woburn, MA, SLM-128). The SLM which induce a individual phase retardation on the pulse spectrum consists of 128 5-mm-high phase-modulating elements with 100- μm width,

and a 2.0- μm gap between adjacent pixels. To achieve minimum aberration and a dispersion less condition, properly aligned the apparatus is required. Optical Pulse will be diffracted by grating and focused by a spherical reflector and propagate into SLM that are Fourier plane, in that we can modulate the phase of frequency domain to achieve our goal. The critical alignment steps are depicted in the following. First of all, let the laser beam go through a BBO crystal to generate a visible second-harmonic beam at 628 nm. Adjusting the red input beam to propagate on a horizontal plane which is parallel to the optical table. Checking out all the diffraction beams propagate on the horizontal plane. The broadband optical spectral components should also spread on the plane. Place the first spherical mirror at approximately one focal length away from the first grating. Rotate the first grating to let the second-order diffracted beam to be centered on the spherical mirror. Make sure that the image is on the SLM plane and all spreading optical spectral components still propagate on the horizontal plane.



Position the second spherical mirror at a distance of $2f$ from the first spherical mirror. Adjusting the angle of the second spherical mirror to let all spectral components approximately overlapped on the position which is similar to first grating of the second grating. Be sure that all beams still propagate on the horizontal plane. Fine tuning the position and the angle of the second grating to let all diffracted spectral components collimate. Finely adjusting the distance between the two spherical mirrors to optimize the output spot for as circular as possible. Make sure the distance between these two spherical mirrors to be $2f$. The output spot shall look like circular in far field. Repeat step until a circular spot in the far field is obtained. Place SLM at approximately the image plane of the first spherical mirror where individual spectral components are focused to their minimum size.

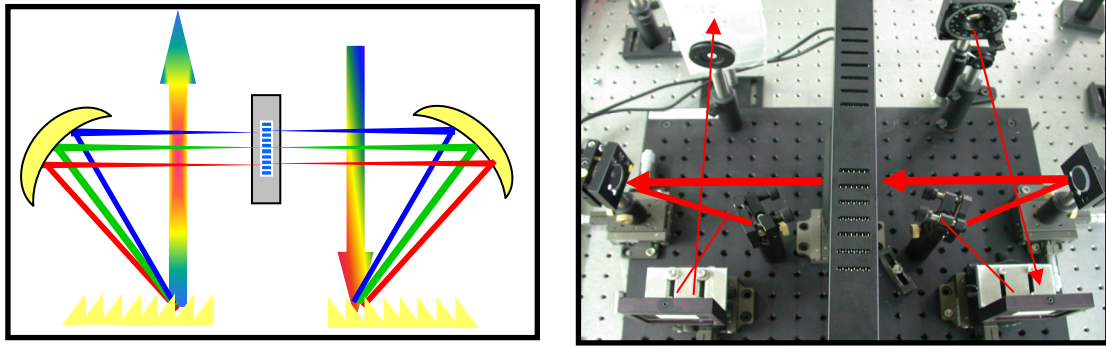


Fig.2-2. The schematic and real setup of our phase-only pulse shaper.

2.2 The Calibration of Spatial Light Modulator (SLM) System

The Spatial Light Modulator -128 modulator arrays provide independent control of each element in a linear array of 128 pixels (SLM-128 models). The pixel array is 5 mm high, and the inter-pixel pitch is 100 microns, resulting in a total array aperture of 12.8 respectively. SLM instruments use special circuitry and timing to ensure the output signal is free from DC content, and for longest life of the liquid crystal optics. The electronics provide up to 10.00V drive with 12-bit resolution, controlled by USB serial interface. The SLM optics use nematic liquid crystal material to alter the phase or polarization state of light. The basic principle is that the crystal material provides an electrically-variable index of refraction for light that is polarized along the crystal's extraordinary axis. **Fig.2-3** show drive level V.S. phase. $V_i = V_{ref} * D_i / 4095$ where V_i is the voltage at pixel element I, and D_i is the digital drive level corresponding to that element. V_{ref} is the reference voltage, 10 V. If the unit is operated as a phase modulator, this is the amount of modulation; or, to convert to express the modulation in radians, $\Gamma = \mu / \lambda$. If the unit is operated as an amplitude modulator, the transmission is $T = \cos^2(\pi, \Gamma)$.

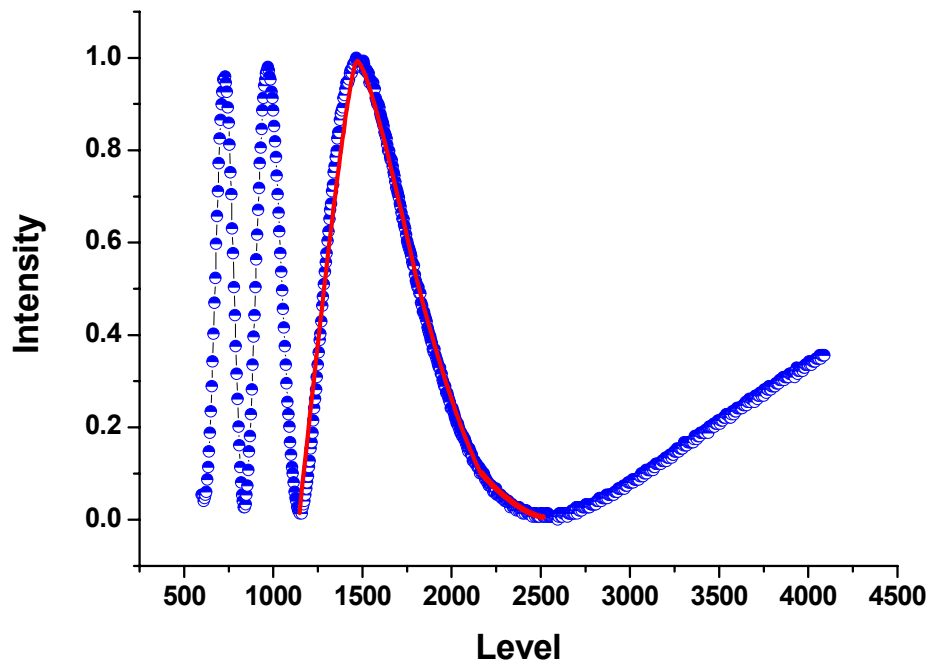


Fig.2-3. The transfer ratio related between level and intensity of laser intensity

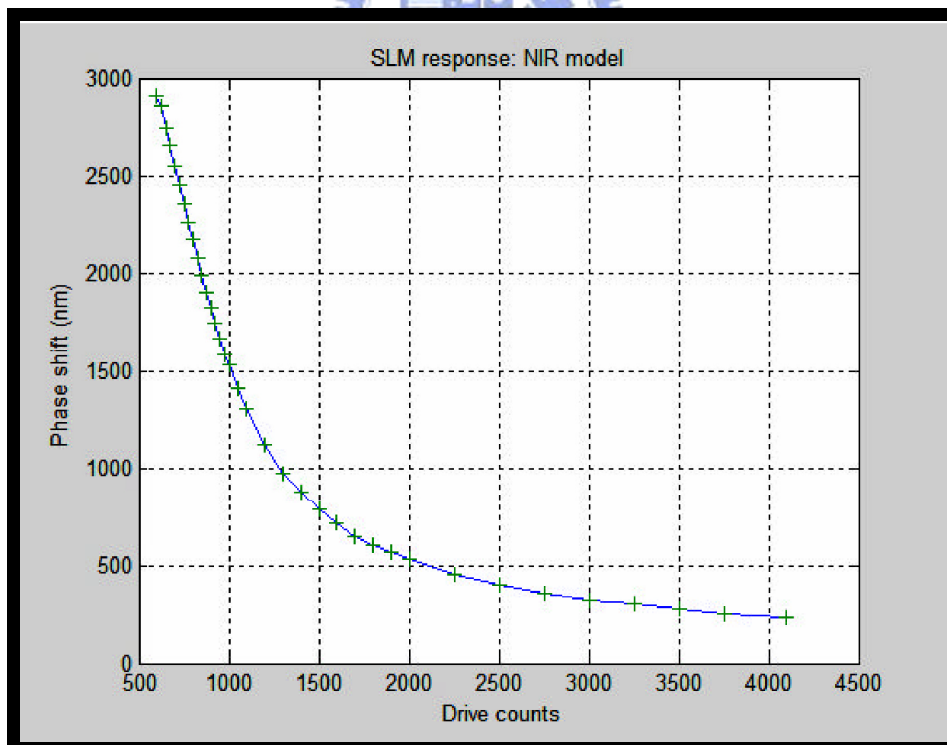


Fig.2-4. Typical modulation transfers function for an SLM with NM wavelength range.

We select the phase retarder curve from red line in the **Fig.2-3** as our database that is the relation between the phase and the level.

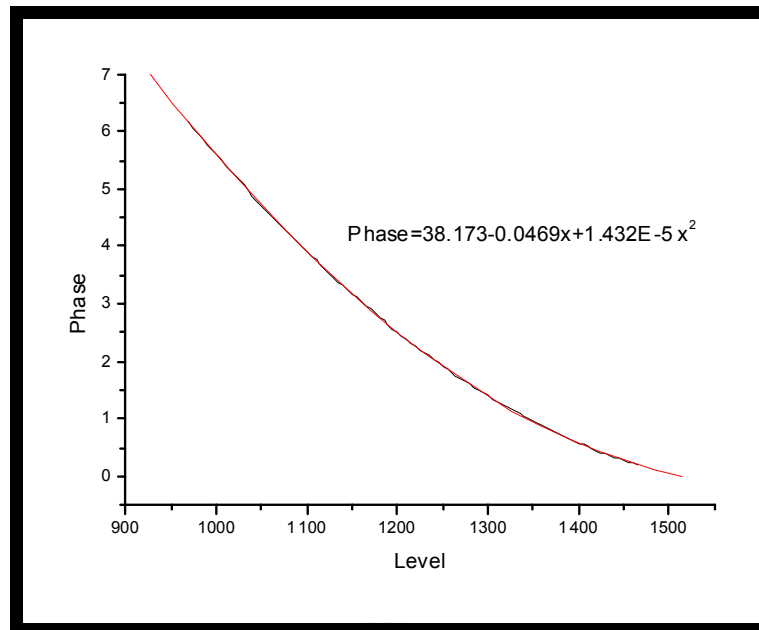
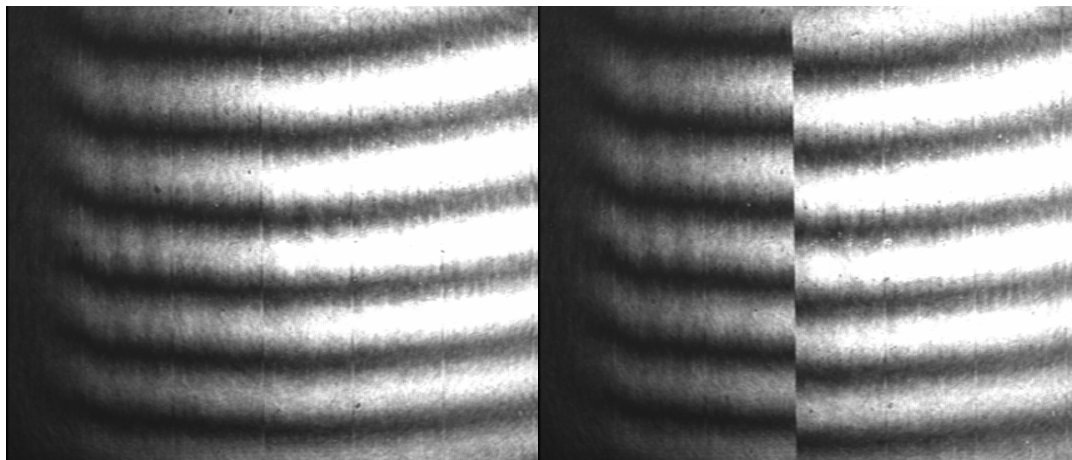


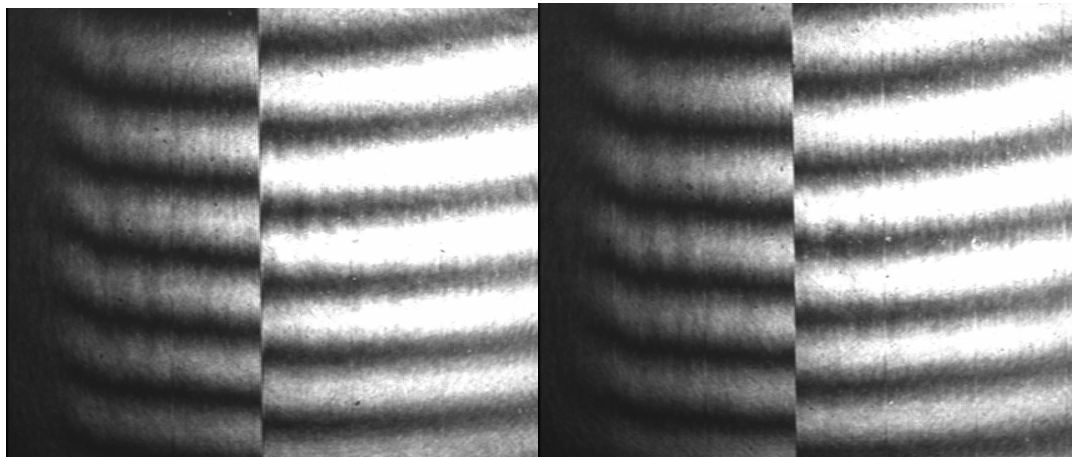
Fig.2-5. The database curve that is the relation between the phase and the level

Because the unequal amplitude of the peaks that Fig.2-3 shows would cause the phase shifted by SLM from 0 to 2π to be inaccurate., we measure phase shift directly by interference method. We use an interferometer and set the SLM to optical path in the one beam of interferometer. We let beam spot cover several pixels of SLM and alter the level (from 970 to 1470) of pixels mantled by laser's spot. Because we devise different phase shift which enable light have different optical distance by SLM in the pixels covered by laser's spot, the outcome of interference will be change. The results of interference can be observed from the **Fig 2-2.5**. We get the image of interference from CCD and design a program by Labview to calculate the image data which have the information about how many phase shifts we add by SLM.



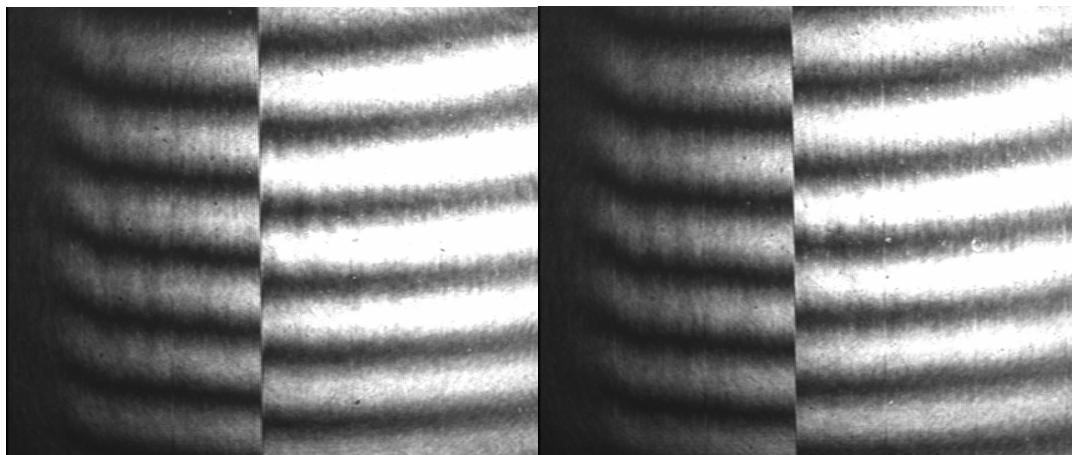
(A) 970

(B) 1010



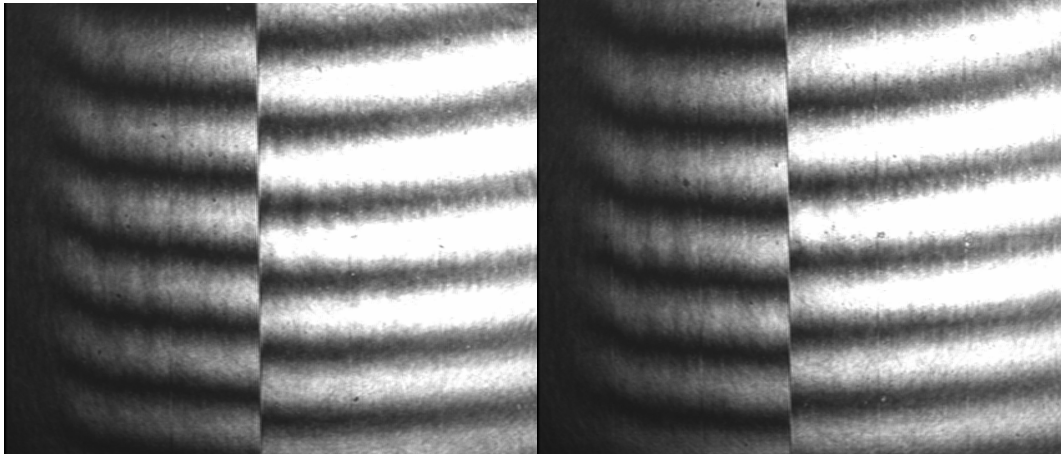
(C) 1050

(D) 1090



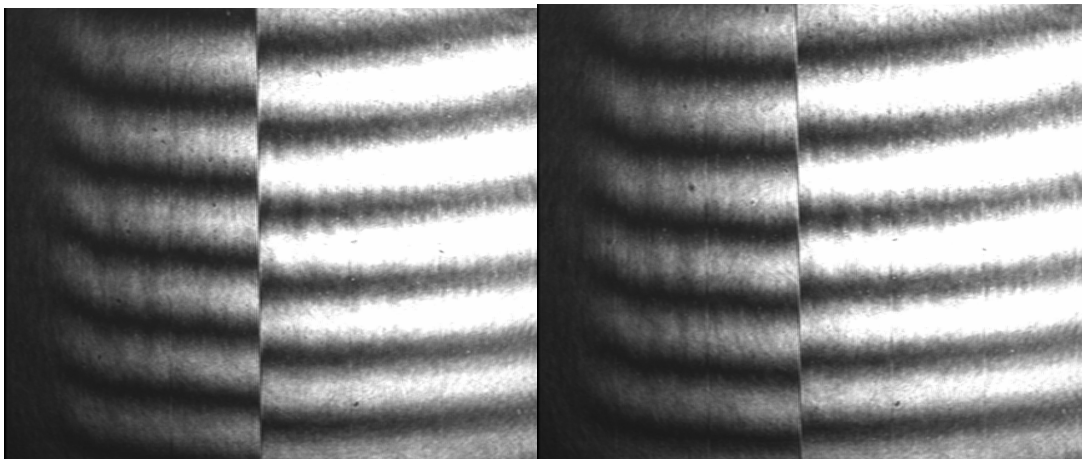
(E) 1130

(F) 1170



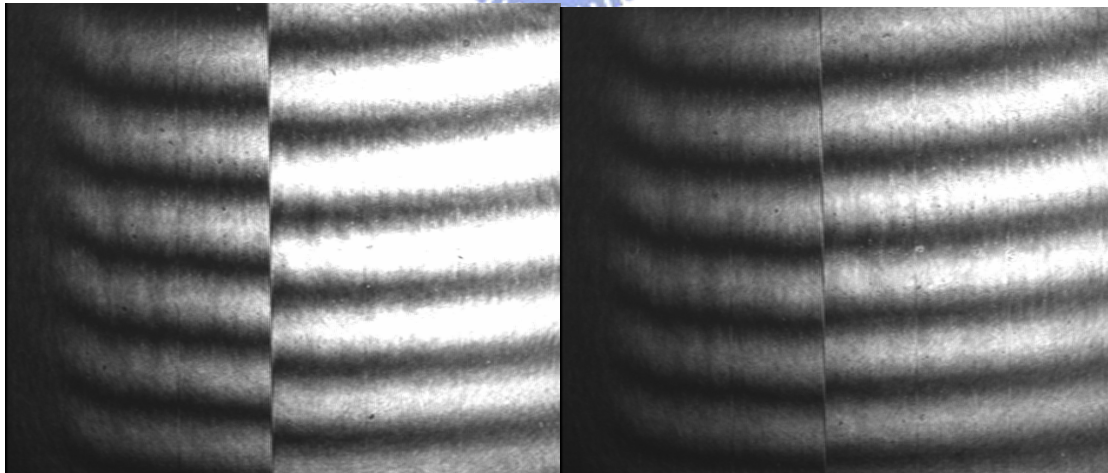
(G) 1110

(H) 1160



(I) 1200

(J) 1240



(K) 1280

(L) 1320

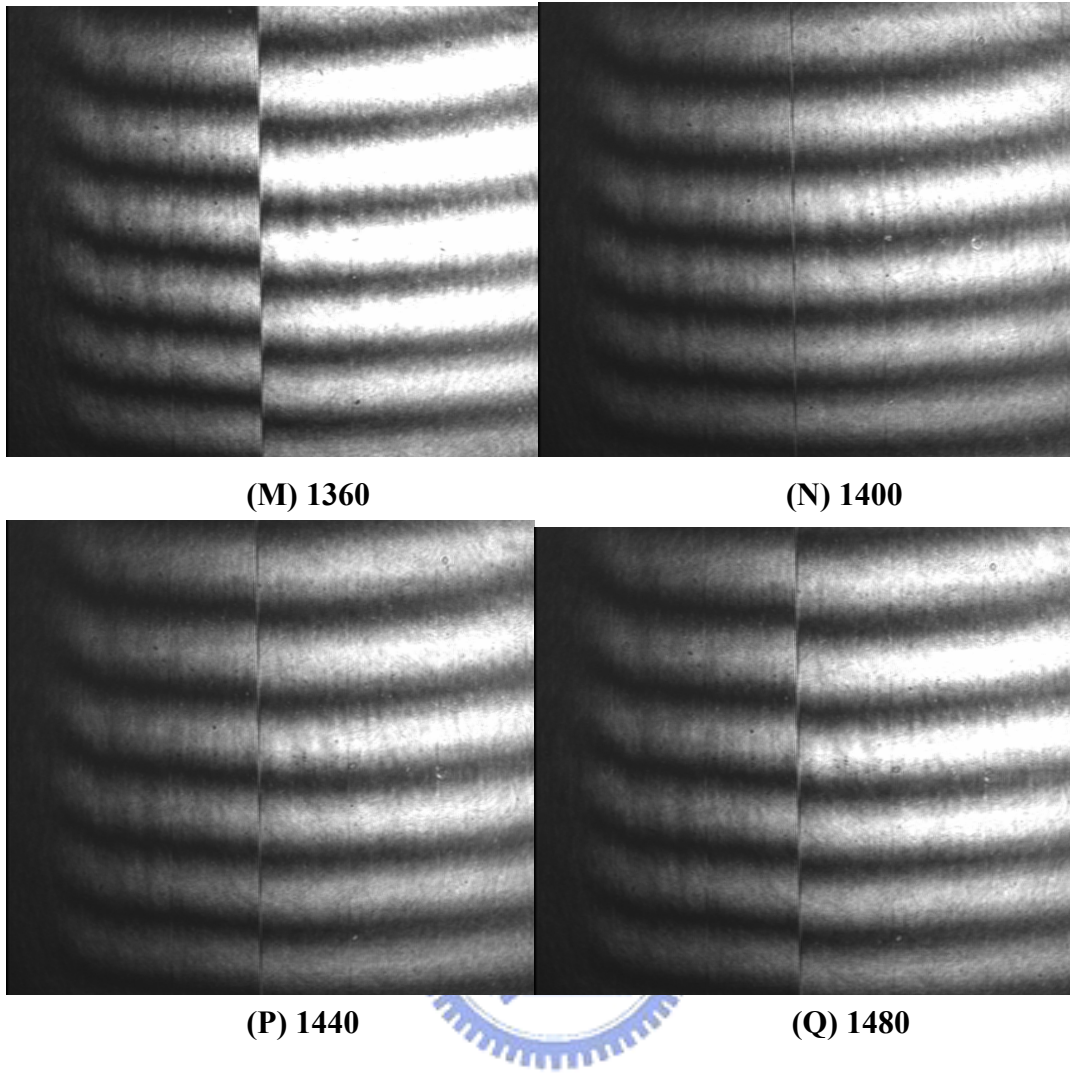


Fig.2.6.The result of interference. The optical distant in the one laser beam of half spot size in interferometric optical path is altered by increase voltage of SLM, and the pixels of SLM increased voltage have different optical distant from that no voltage increased. The Figs show the phenomenon which the voltage is raised from 970 to 1480 showed in figure (A) to figure (Q). The optical distant are increased gradually, the interferometric fringes are shifted. So we use the image data to calculate the relation between increased voltage of pixel and phase shifted value SLM induced.

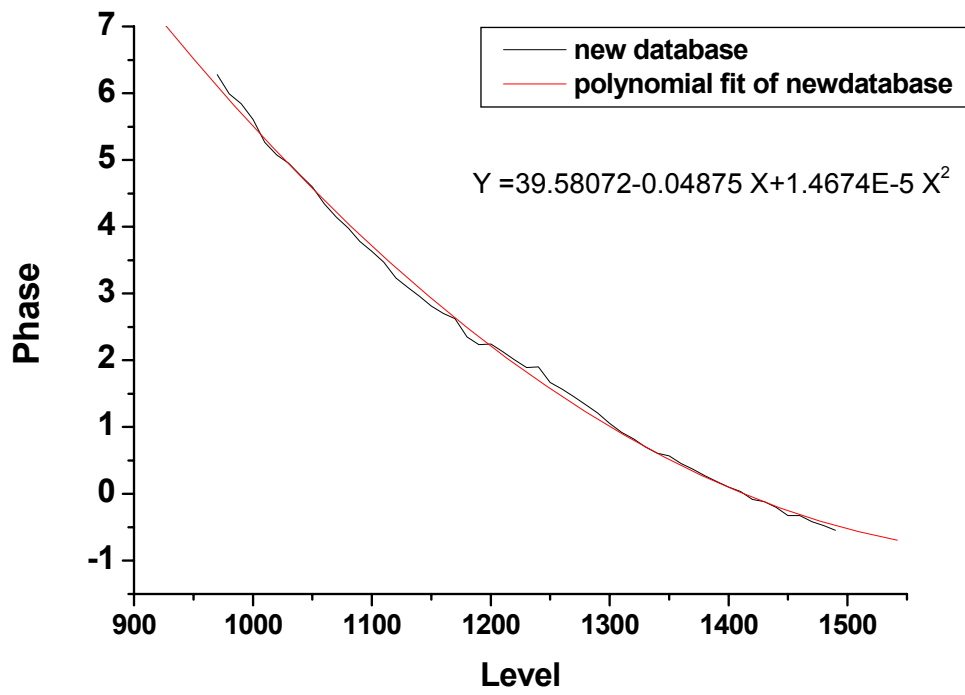
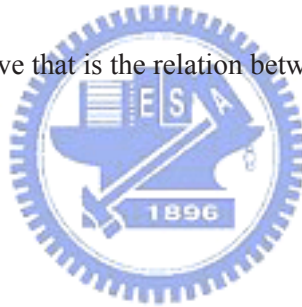


Fig.2-4 The database curve that is the relation between the phase and the level




Chapter3. Synthesis of Femtosecond Optical Pulses

Shaping of ultrashort optical pulses into desired waveforms has been a subject of extensive work in recent years [9-15]. The most successful techniques for ultrashort pulse shaping involve Fourier synthesis, where the optical field is modified by filtering of its spatially dispersed frequency components. Dynamic computer controlled pulse shaping was achieved by liquid-crystal modulators [8]. Pulse shaping system demonstrate the Fourier spectral filter that was calculated by fully characterized input pulse cause the output laser to match a desired, well-defined waveform. However, in some situations the optical field to be used for an experiment is difficult or even impossible to be determined before hand, and consequently, the corresponding spectral filter cannot be calculated. In other situations the performance of these pulse shapers is limited by the need to constantly update the spectral filter in order to account for variations of the laser source. These limitations can be overcome by use of an adaptive approach [16-17]. The Fourier filters needed to generate the desired field for specific tasks cannot be directly computed. In this chapter, we use SLM to manipulate the phase of frequency domain and adaptively reduce pulse width where the phase are all in phase then let laser pulse to arrive transform-limited. Transform-limited approach is a very important process in adaptive pulse synthesizer. Since phase-only shaping is not capable of absolutely arbitrary shaping, an approximate method was used implemented using the Gerberg-Saxton (GS) algorithm[6]. Based on the input pulse spectrum and the intensity target in the time domain, this algorithm computes the desired spectral phase profile which yields the best approximation of the target waveform. We used a programmable pulse shaper

that allows for independent control of the individual spectral components of the incoming pulses, to realize almost arbitrary waveforms.

This Chapter is organized as follows. We introduce in section 3-1 our laser system. Section3-2 describes adaptive pulse shaping with freezing phase scheme and our experimental setup, results. In Section3-3, we present several examples of synthesis femtosecond optical pulses with Gerchberg-Saton algorithm. Finally, Section 3-4, we control the chirp of pulse by using phase-only optical pulse shaping system.

3-1.Mode-locked Ti: sapphire Laser



The Ti: sapphire femtosecond laser system from Spectra Physics company , which can generate ultrashort optical pulses in near infrared ($\lambda \sim 800$ nm). The laser is self mode-locked by keeping lasing longitudinal cavity modes in phase to produce ultrashort near transform-limited optical pulses with pulse duration about 27 fs. The Ti: sapphire oscillator gives pulses with a typical full-width-at-half maximum (FWHM) bandwidth of about 40 nm at a repetition rate of 80 MHz and average power 450mW. The ultrashort pulse duration can yield an enormous peak power density after focusing. The Ti: sapphire laser is pumped by a5-W diode laser.

3-2.Adaptive Pulse Shaping with Freezing Phase Scheme

(I) Theory:

We can first express optical field in terms of its spectral components in SLM of 128 pixels instead of the freezing phase scheme as formula as follow:

$$E(t) = \sum_{n=1}^{128} A_n \exp[i(w_0 + n\Delta w) + \phi_n];$$

Where Δw is the width of spectral components involved in the coherent pulse, ϕ_n and A_n denote the phase constant and amplitude of each spectral component, and w_0 is the optical carrier frequency.

The pulse spectrum is diffracted by a pair of grating in the phase-only pulse shaping system, so 128 pixels of SLM can be used to mean a phase retardation pattern $\{\Theta\}$ on the optical spectrum and transforms the unshaped coherent field into a shaped field as equation as follow:

$$E(t) = \sum_{n=1}^{128} B_n \exp[i(w_0 + n\Delta w) + \phi_n + \Phi_n];$$

After propagating through a pulse shaping system, A_n / B_n denotes the field transmittance of the n th pixel. If the constant phase $\phi_n + \Phi_n$ is equal to zero, the shortest pulse and consequently the highest peak intensity are produced. In other word, it indicates that the peak amplitude of the shaped field $E(t)$ can reach a maximum value when $\phi_n = -\Phi_n$.

In brief our algorithm can first divide the elements of SLM into two groups

$$E(t) = \sum_{n=1}^{64} B_n \exp[i(w_0 + n\Delta w) + \phi_n + \Phi_n];$$

$$E(t) = \sum_{n=64}^{128} B_n \exp[i(w_0 + n\Delta w) + \phi_n + \Phi_n];$$

The second-harmonic (SH) signal generated from a nonlinear optical crystal with the optical coherent pulse. We can represent the physic model as mathematical equation.

$$\begin{aligned} |E|^4 &= B_1 \exp(i\theta_1) + B_2 \exp[(i\theta_2 + \psi)] \\ &= \{|B_1|^2 + |B_2|^2 + |B_1|^* |B_2|^* \cos(\theta_1 + \theta_2 + \psi)\}^2 \end{aligned}$$

If we let $(\theta_1 + \theta_2 + \psi)$ equivalent to zero by changing phase of one group, second-harmonic signal can be achieved maximum value. In other words, SLM can be used to make those two spectral groups in-phase.

To further illustrate the freezing phase procedure, we use four phasors to represent the spectral phase profile of a coherent optical pulse. The optical field can therefore be simplified as $E(t) = \sum_{G=1}^4 A_G \exp(i\phi_G)$. To freeze the spectral phases, we first pick up a spectral component and align the phasor with the summed direction of the rest spectral components by using SLM to introduce a compensation phase. We can combine $A_1 \exp(i\phi_1)$, $A_2 \exp(i\phi_2)$, $A_3 \exp(i\phi_3)$ into the reference group and let $A_4 \exp(i\phi_4)$ to vary. The same procedure is repeated on group 1, 2, and 3. In final state, four groups are all in phase.

(II) Experiment:

Fig. 3-1 presents the schematic of an adaptive pulse shaping apparatus¹⁹ used in this study. The laser system is a mode-locked Ti: sapphire laser pumped by a diode-pumped. A typical output of the mode-locked Ti: sapphire laser was 450 mW of average power at a repetition rate of 80 MHz with a 5-W pump. The central wavelength is 800nm, and a typical full-width-at-half maximum (FWHM) bandwidth

was approximately 40 nm, corresponding to 40-fs pulse duration.

The pulse is tailored by a pulse shaper consisting of a pair of gratings (600 g/mm), two concave reflectors with a focal length of $f=20$ cm, and a liquid crystal SLM (Cambridge Research and Instrumentation Inc. (CRI) Woburn, MA, SLM-128). The SLM consists of 128 5-mm-high phase-modulating elements with 100- μm width, and a 2.0- μm gap between adjacent pixels. After reassembled by the output grating, the shaped pulse is focused onto a sample under test. The phase distortion in the reflected optical pulse can be pre-compensated by the SLM. An optical pulse with constant phase can therefore be yielded before a 3-mm thick BBO second harmonic generation (SHG) crystal. Note that transform-limited pulse with constant phase can produce a maximum second-harmonic (SH) signal from a transparent nonlinear optical crystal. We therefore combine BBO SHG with a photodiode to offer a functionality of constant phase detection. The photodiode signal is sent to a computer for generating phase compensating pattern with the freezing-phase algorithm. **Fig. 3-2** shows the Flow chart depicts the procedure used to implement the freezing-phase scheme into the theoretical and experimental studies

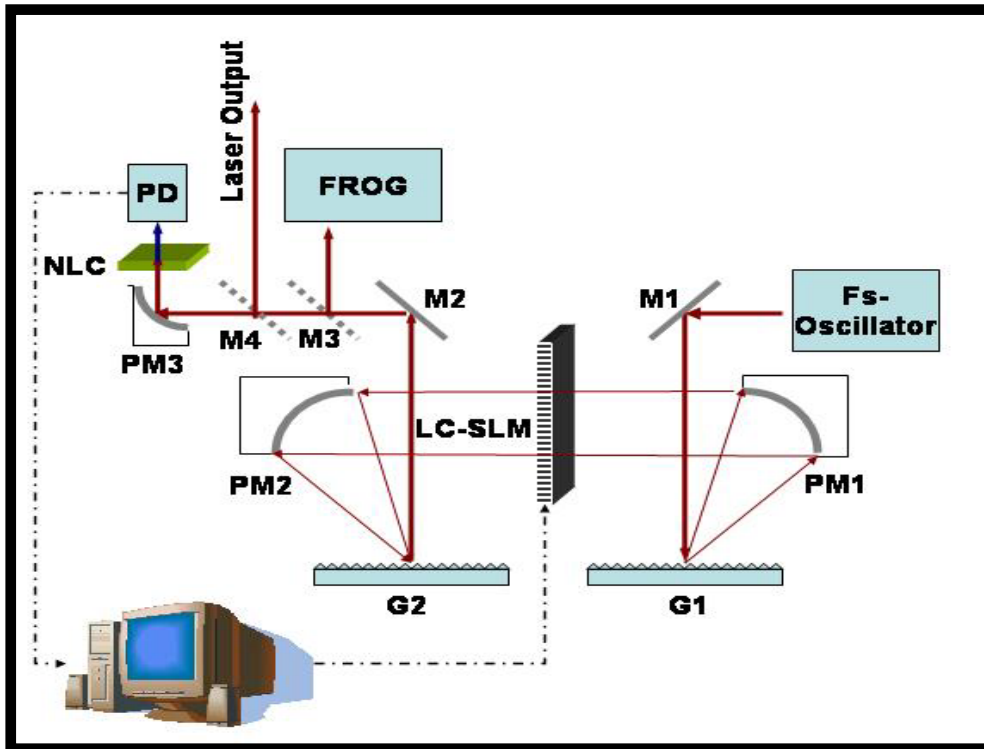


Fig. 3-1: Schematic of the adaptive coherent control system with an all reflective 4-*f* pulse shaper used in this study.

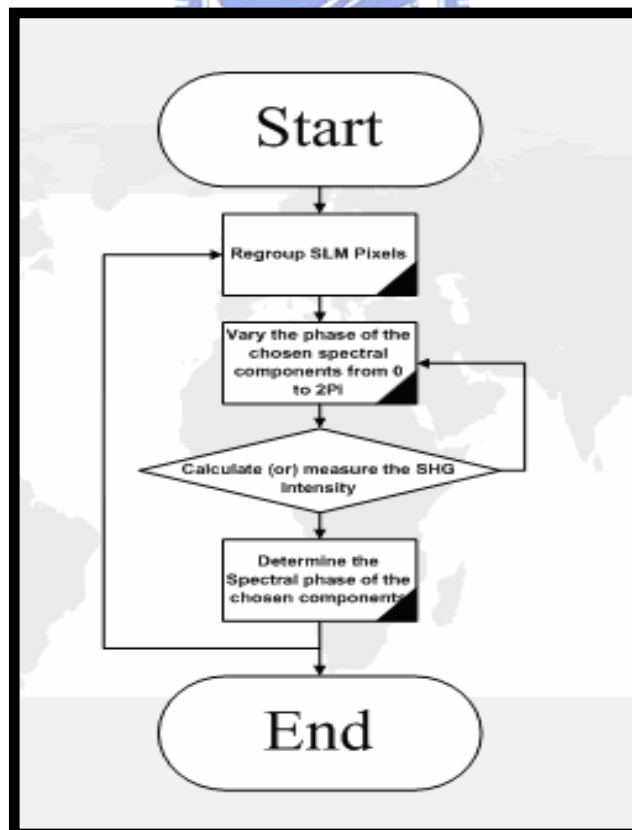


Fig. 3-2: Flow chart depicts the procedure used to implement the freezing-phase

scheme into the theoretical and experimental studies

An experimental verification of the new freezing phase scheme starts with grouping of the SLM pixels into two classes: the first group plays the role of phase modulation. The other group, which contains the rest pixels, is used as the reference. We vary the phase of the modulation group from 0 to 2π to maximize the SH intensity. The procedure repeats by regrouping the SLM pixels until the phase retardations of all pixels are adjusted. **Fig. 3-3** shows adaptive phase added on liquid crystal spatial light modulator for various stages. Because transform-limited approach is a very important process in adaptive pulse synthesizer, we make the laser transform-limited by the method and measure the laser pulse width with autocorrelator and FROG. **Fig. 3-4** shows transform-limited Autocorrelation trace after freezing, pulse width can reduce to 27fs. **Fig. 3-5** show retrieved amplitude and phase of pulse, checked with typical 64x64 SHG FROG, after freezing. The figure shows the phase of pulse is in phase.

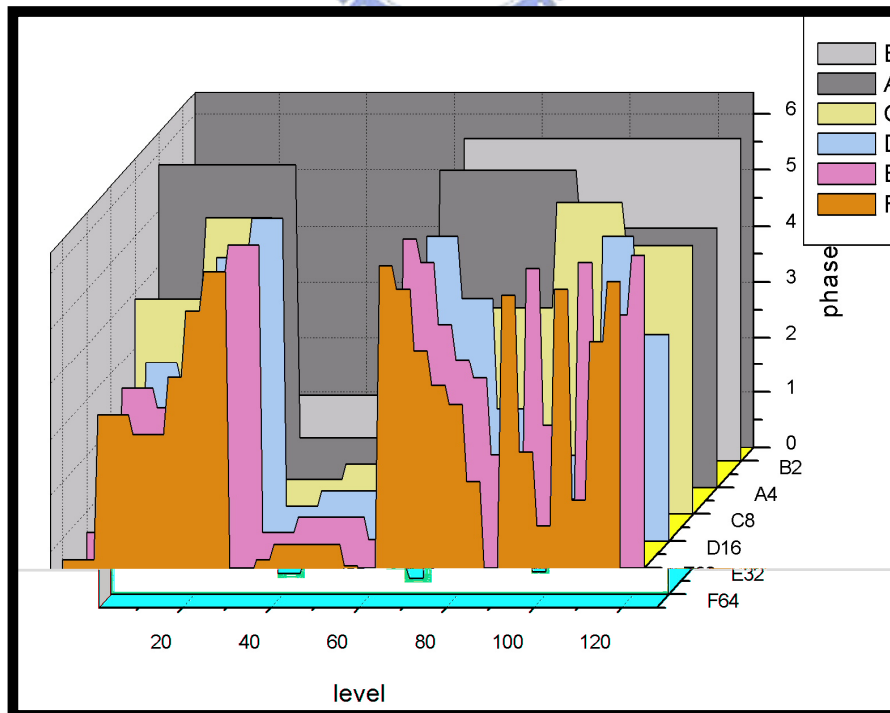


Fig 3-3 Adaptive phase added on liquid crystal spatial light modulator for various

stages

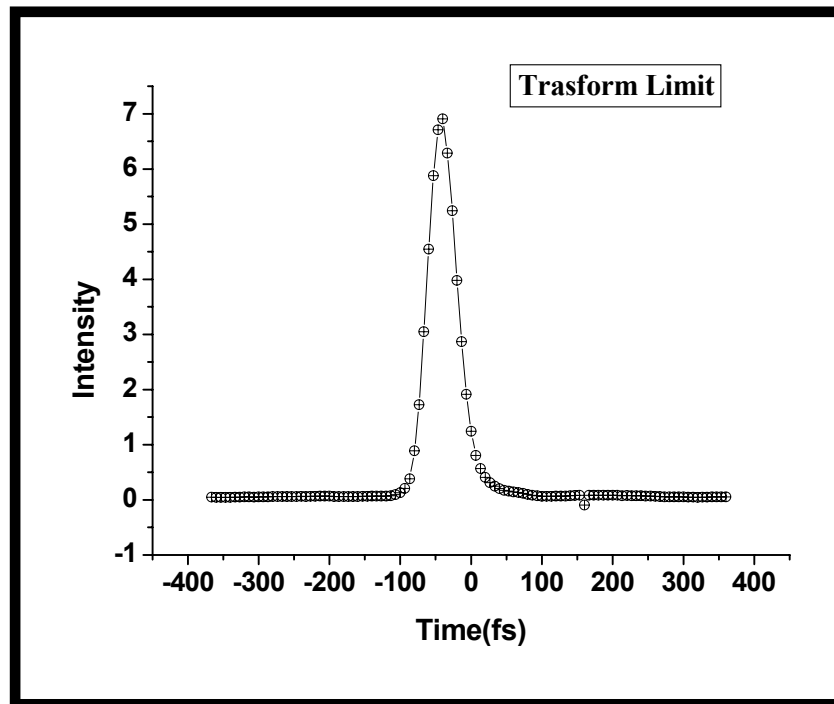


Fig. 3-4 Transform-limited Autocorrelation trace after freezing

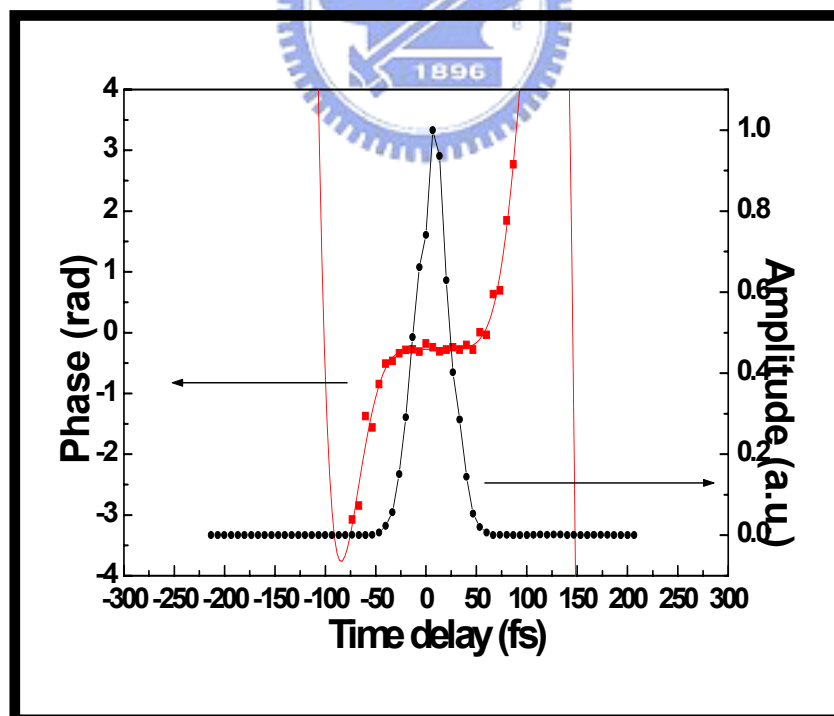


Fig. 3-5 Retrieved amplitude and phase of pulse, checked with typical 64x64 SHG FROG [18], after freezing.

3-3.Synthesis of Femtosecond Optical Pulses with Gerchberg-Saton Algorithm

(I) Theory:

Since phase-only shaping is not capable of absolutely arbitrary shaping, an approximate method was used implemented using the Gerberg-Saxton (GS) algorithm. After freezing scheme and achieve the transform-limited pulse, we calculate the desired phase mask with Gerchberg-Saton algorithm. Based on the input pulse spectrum and the intensity target in the time domain, this algorithm computes the desired spectral phase profile which yields the best approximation of the target waveform. Although other algorithms, such as the genetic algorithm, can be used to compute the phase masks, the GS was shown to yield good results with near-real time performance and it is simpler to implement and operate. The GS algorithm finds a particular spectral phase function which, when combined with an input intensity spectrum which shows, will yield a shaped temporal intensity profile as close to the target as possible. On each iteration the GS algorithm makes use of two constraints (invariants) of the problem in two conjugate domains: (i) the input pulse spectrum, unaffected by phase filtering, and (ii) the temporal intensity target. Initially the pulse spectrum is Fourier-transformed into the time domain, assuming a random phase, where the amplitude is replaced with the target while the phase is retained. Fourier transform back to frequency domain is then performed where the spectral amplitude is replaced with the input pulse spectrum and the phase is again retained without change. The procedure is repeated until the deviation between the amplitude of the desired pulse $\{ \sqrt{I(t)} \}$ and temporary field $\{|E(t)|\}$ as small as possible. On the last

iteration this phase constitutes the desired phase mask. In mathematical notation, for the k th iteration this can be expressed as

$$E_{k(t)} = |E_k| \exp[i\phi_k(t)] = FFT^{-1} \{ \bar{E}_k(w) \} \dots\dots\dots (1)$$

$$E'_{k(t)} = |E_{tar}(t)| \exp[i\phi_k(t)] \dots\dots\dots (2)$$

$$E_k(w) = | \bar{E}'_k(w) | \exp[i\phi'_k(w)] = FFT \{ \bar{E}'_k(t) \} \dots\dots\dots (3)$$

$$\bar{E}_{k+1}(w) = | \bar{E}_{meas}(w) | \exp[i\phi_{k+1}(w)] \dots\dots\dots (4)$$

Where $\phi_{k+1}(w) = \phi'_k(w)$ is the new spectral phase, $\bar{E}'_k(t)$ is an estimate of the target, and $\bar{E}_k(w)$ is an estimate of the measured intensity spectrum. Typically, the algorithm converges in a few iterations, although several hundred iterations are sometimes required for complex target waveforms. **Fig.3-8** shows us the flow chart of GS algorithm.

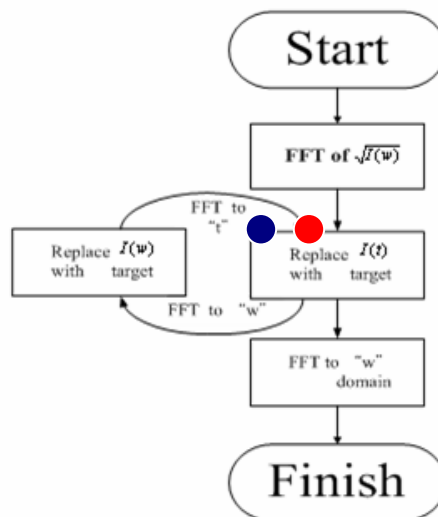


Fig.3-8 The flow chart of GS algorithm. ● Start point. ● Stop point

(III) Simulation of Gerberg-Saxton algorithm

To implement the algorithm successfully, we have to measure the spectrum of the input laser pulse as the first step. The figure of spectrum shows in **Fig. 3-9**. We design the waveform of laser pulse which apply to our physic model, and initially guess the random phase mask of spectrum to execute GS algorithm. Finally, we terminate GS algorithm until the deviation between the target we design and the temporary filed calculated at the blue point in **Fig. 3-8** is less than an error upper limit. **Fig. 3-10** shows the four examples calculated from GS algorithm. **Fig 3-10.(a)(b)(c)** display the GA results when the target pulses are one peak ,two peaks, square pulse. **Fig. 3-11** shows the convergent time of the error of square pulse. On the whole, the whole procedures can be achieved within about one minute to yield the desired spectral phase profile. We use C language to program the GS algorithm. By using an initial random phase pattern, GSA achieves the target pulse faster as compared to that using an initial constant phase pattern.

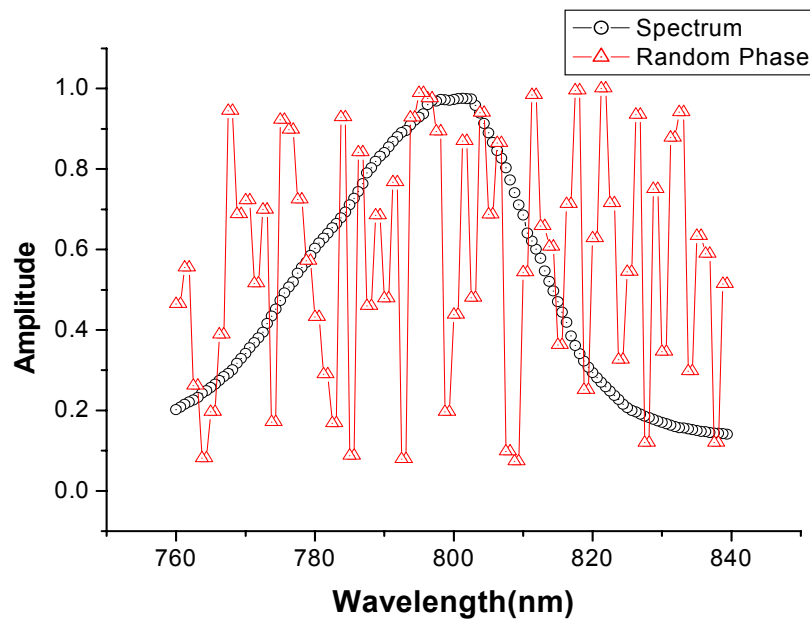


Fig.3-9 The spectrum of laser

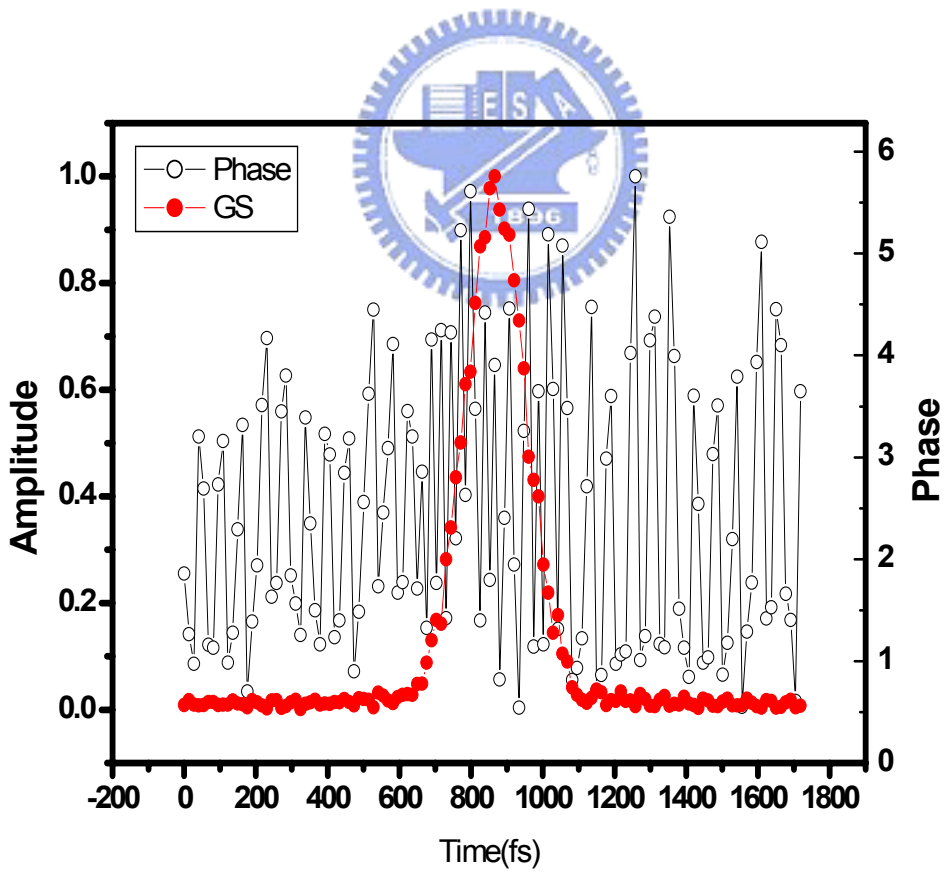
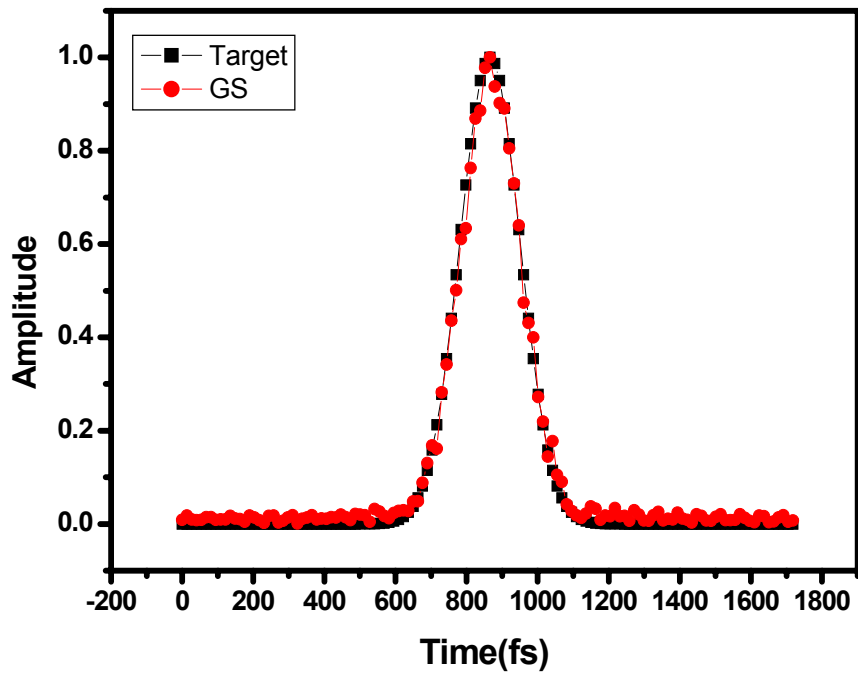


Fig 3-10. (a) The GS results of simulated one pulse (pulse width is 169fs) and it's the phase.

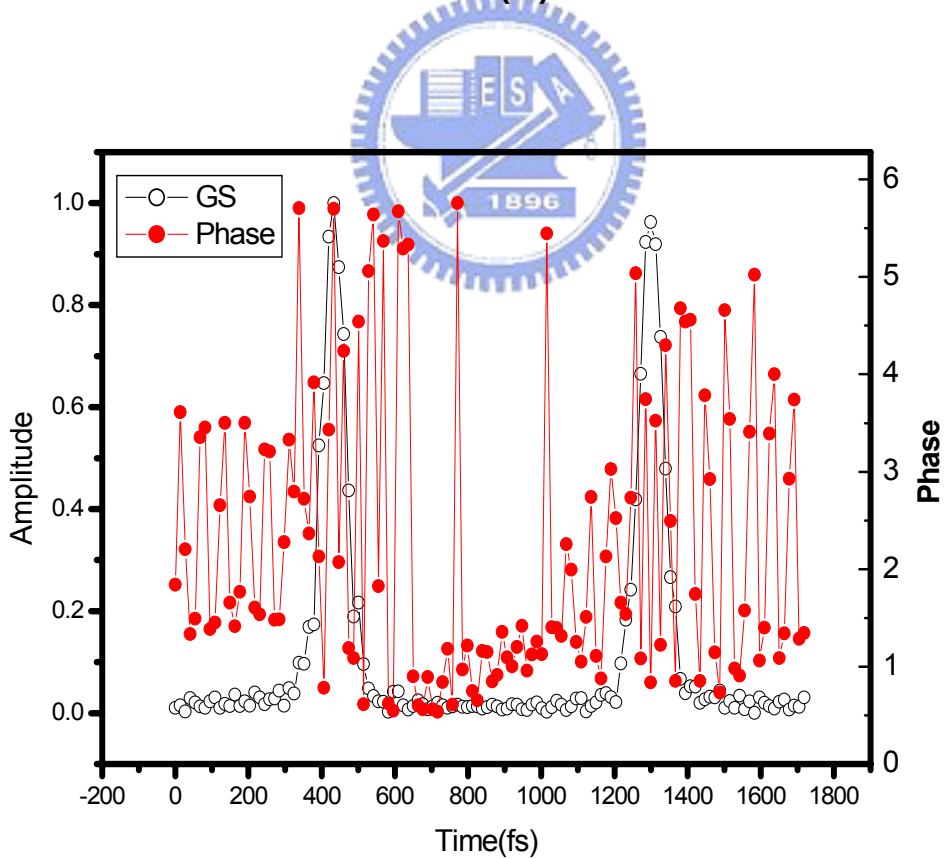
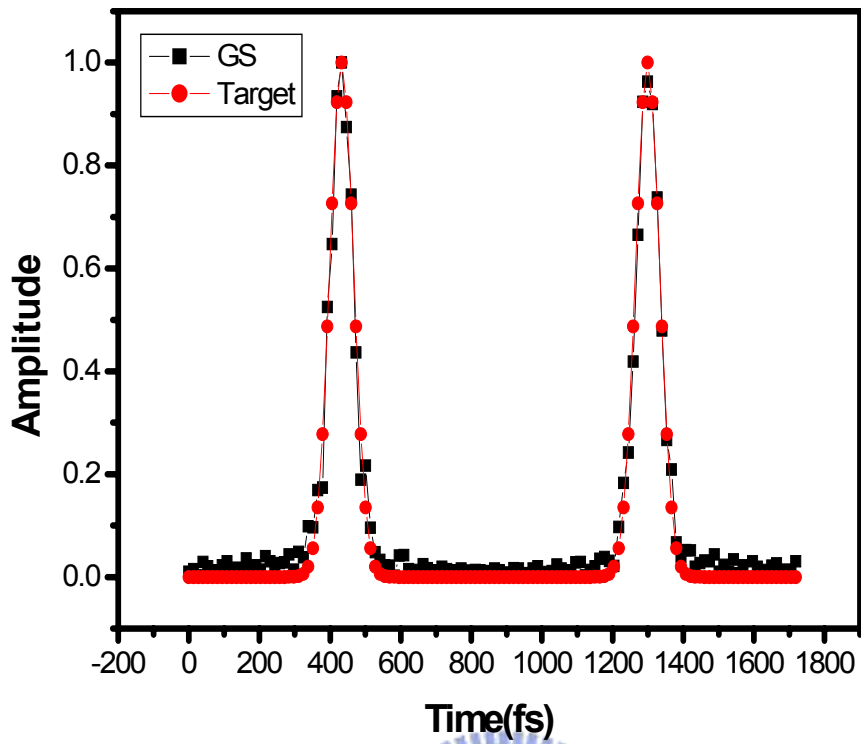


Fig 3-10. (b) The GS results of simulated two peaks pulse (pulse spacing is 836fs) and it's the phase.

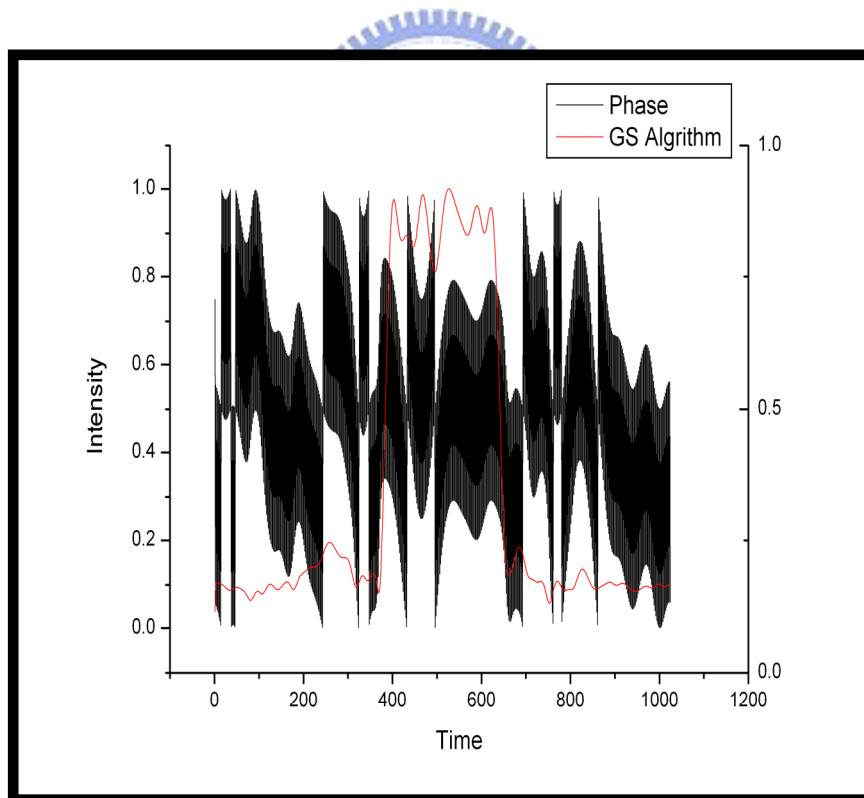
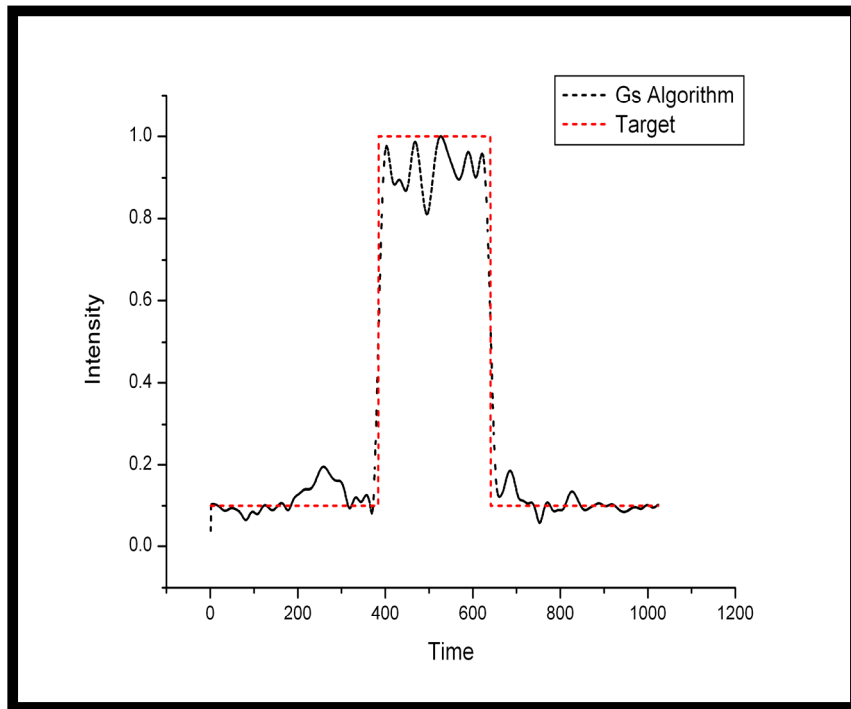


Fig 3-10. (c) The GS results of simulated square pulse and it's the phase.

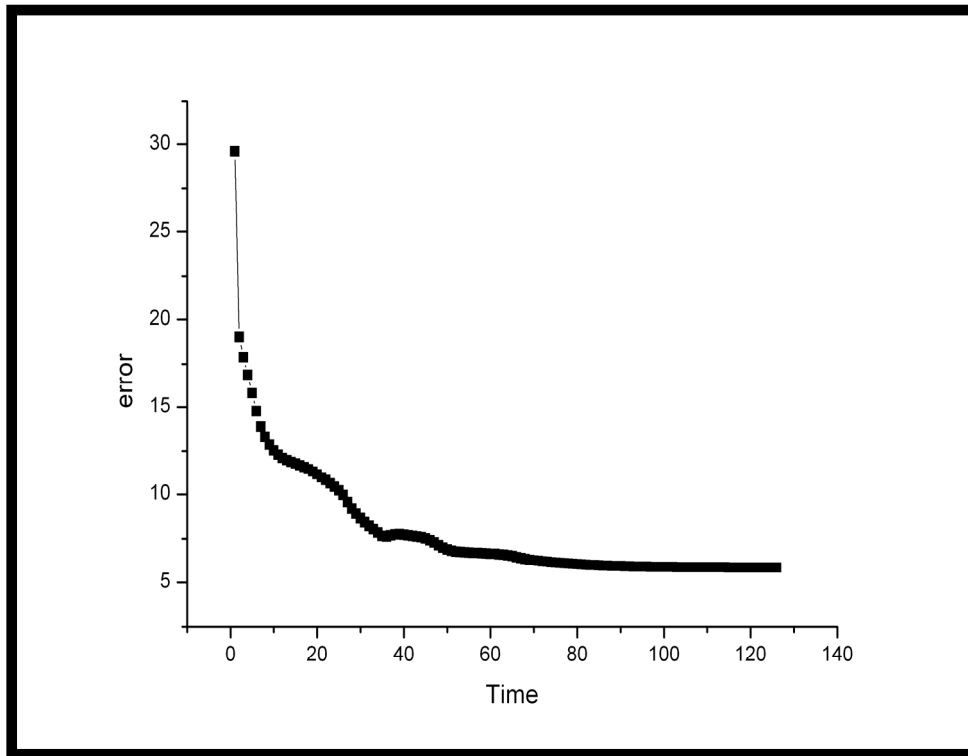


Fig 3-11. The convergent time of square pulse.



(IV) Experimental results

Experimental results of Gs algorithm was measured by autocorrelator, the optical phase retardation patterns obtained from GSA were uploaded to our phase-only pulse shaper with an LC SLM-128 in the Fourier plane. The output pulse from the shaper is brought to a home-made intensity autocorrelation setup. **Fig 3-12.(a)(b)(c)(d)** display the GA experimental results of autocorrelation traces when the target pulses are two peaks positioned at different pulse spacing on the time axis: (a) 214fs, (b) 300fs (c)380fs (d)560fs. **Fig 3-13.(e)(f)** represent the results of autocorrelation traces from GA when the target pulses are multi-pulse at different pulse spacing on the time axis: (e)eight pulses, pulse spacing 188fs, (f)ten pulses, pulse spacing 180fs.

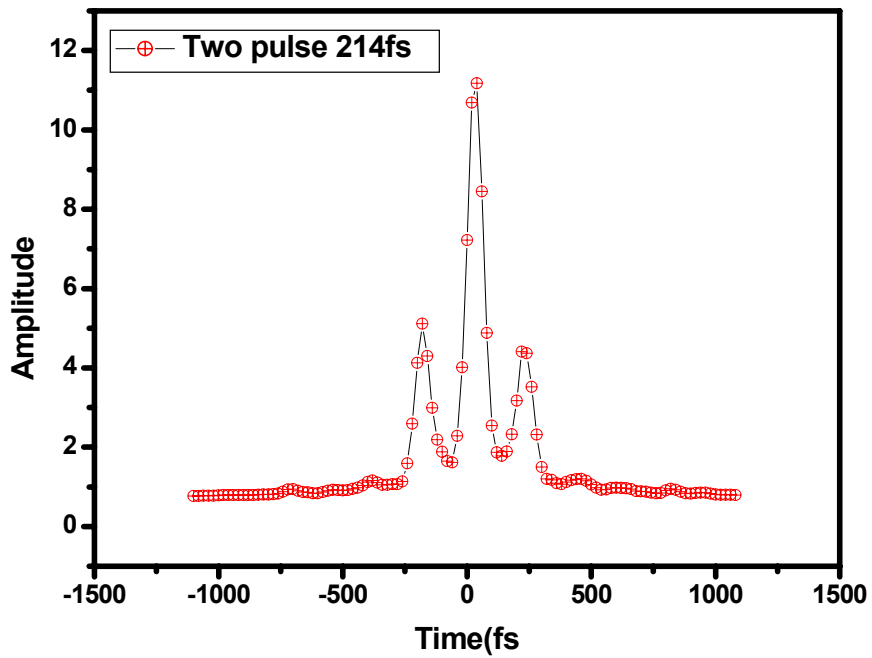


Fig 3-12.(a) display the GA experimental results of autocorrelation traces which experimental spacing is 214fs (theory spacing is 201fs).

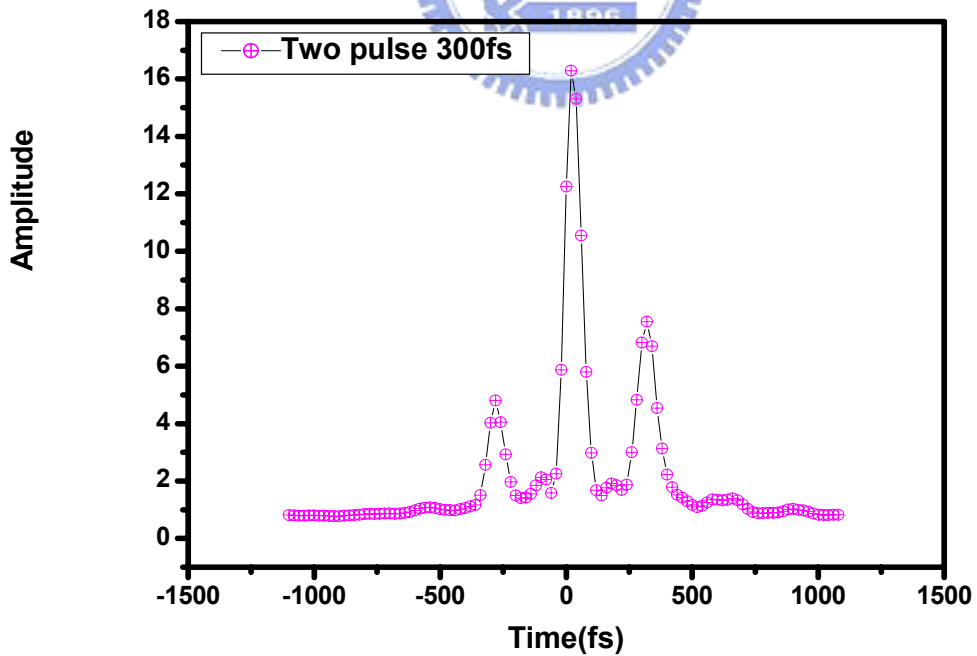


Fig 3-12.(b) display the GA experimental results of autocorrelation traces which experimental spacing is 300fs (theory spacing is 290.16fs).

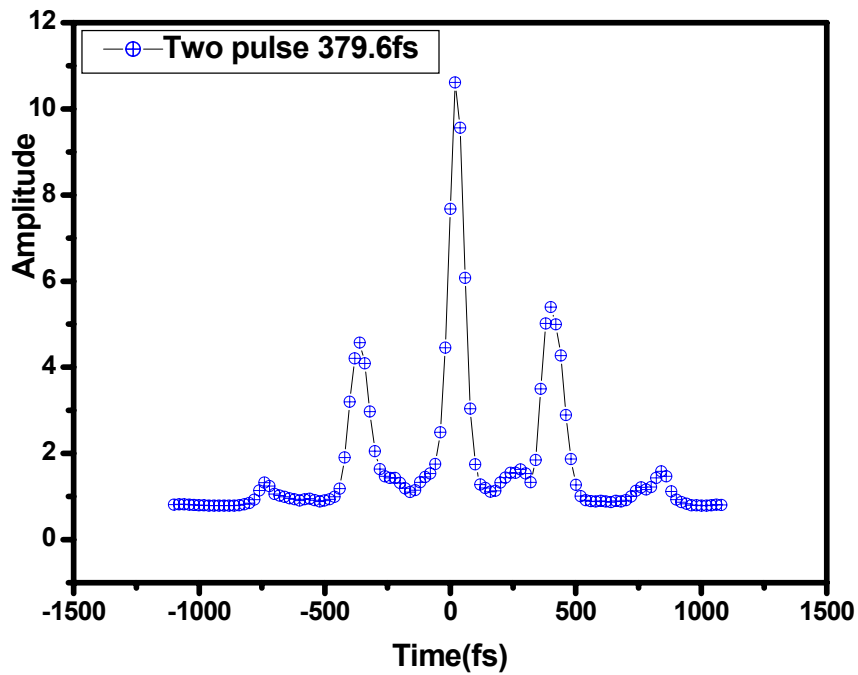


Fig 3-12.(c) display the GA experimental results of autocorrelation traces which experimental spacing is 379.6fs (theory spacing is 379.44fs).

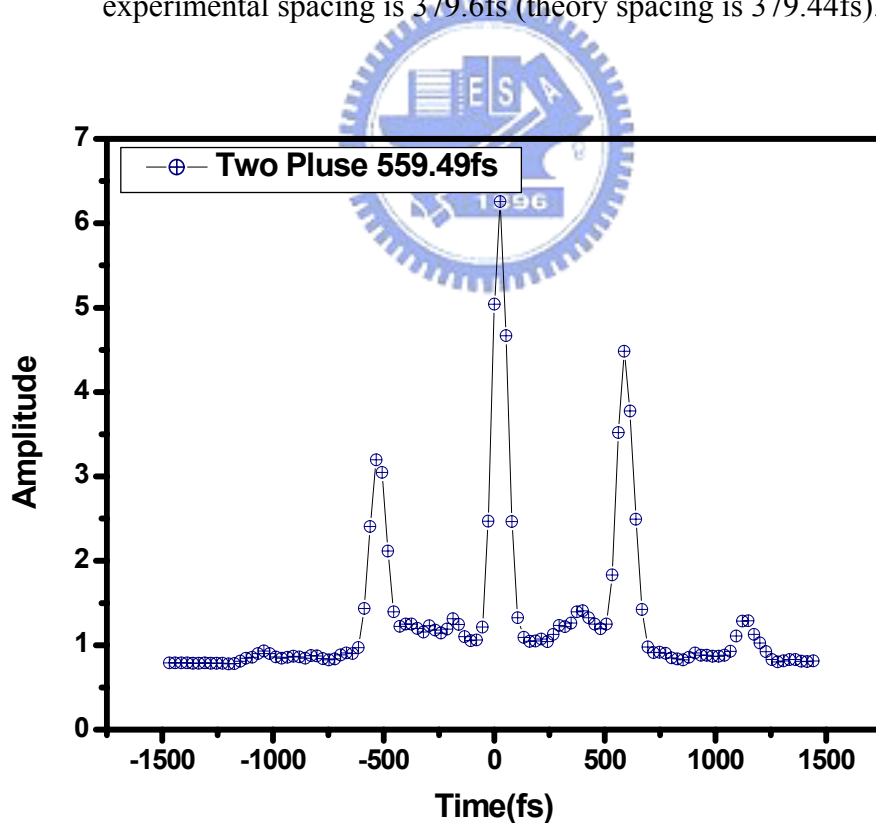


Fig 3-12.(d) display the GA experimental results of autocorrelation traces which experimental spacing is 559.49fs (theory spacing is 513.36fs).'

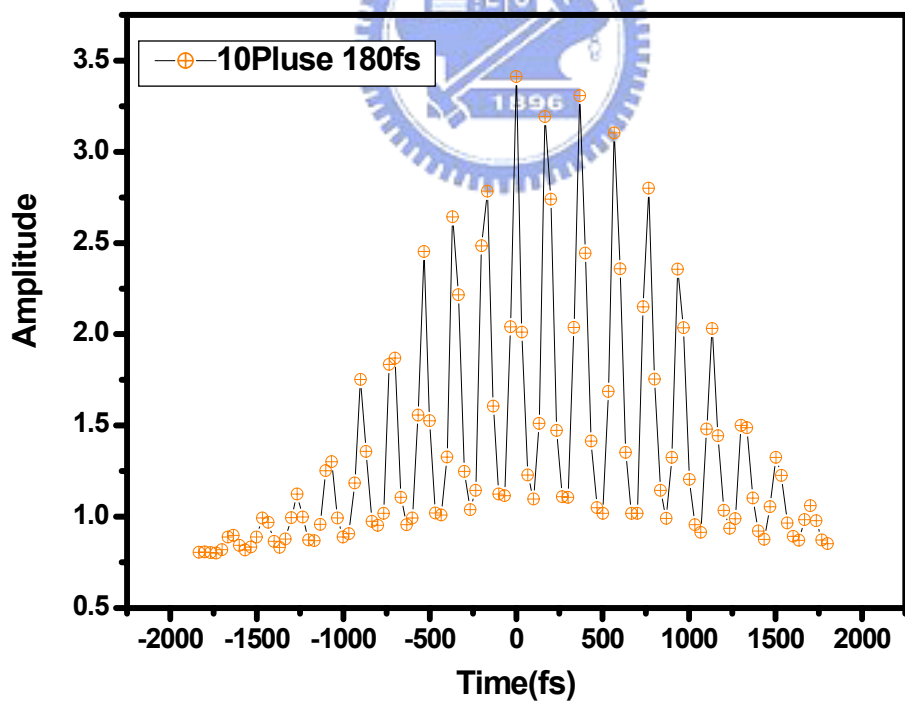
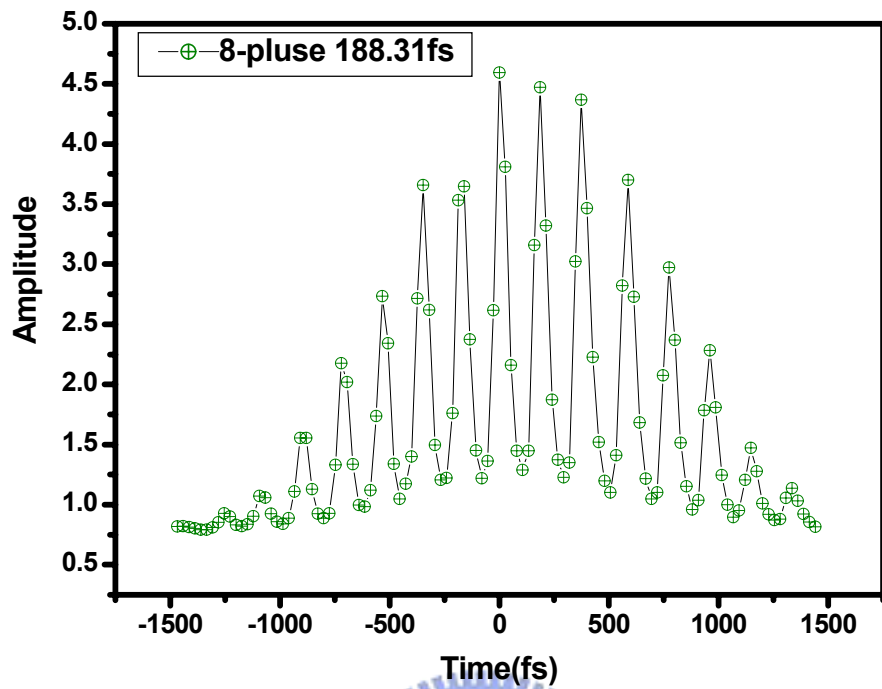
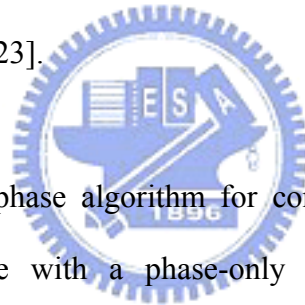


Fig 3-13.(e)(f) represent the results of autocorrelation traces from GA when the target pulses are multi-pulse at different pulse spacing on the time axis: (e) eight pulses, pulse spacing 188fs, (f) ten pulses, pulse spacing 180fs.

Chapter4. The Application of Pulse Shaping in THz Waveform Synthesis

In the above-mentioned of the thesis, we demonstrate the optical synthesis technique for a desired ultrafast optical pulse with Gerchberg-Saxton (GS) algorithm. GS achieves the optical waveform we design. Base the algorithm, multi-pulse with different pulse duration, two pulses with dissimilar pulse duration and single pulse using unlike phase pattern to achieve different pulse width can be accomplished. Pulse shaping technology has already demonstrated a strong impact as an experimental tool providing unprecedented control over ultrafast laser waveforms for THz waveform synthesis [18-23].



We use a new freezing phase algorithm for complete-field characterization of femtosecond ultrashort pulse with a phase-only pulse shaping apparatus. The operational principle is based on the fact that the highest peak intensity corresponds to a complete frozen-phase state of all spectral components. Our experimental and theoretical results reveal several unique features and advantages. We will illustrate this technique using several experimental examples, including manipulation of the bandwidth and the pulse number of ultrafast terahertz waveforms as well as generation of different terahertz spectrum.

This Chapter is organized as follows. We introduce in section 4-1 the principle of THz radiation. Section 4-2 describes Simulation of THz Radiation from biased photoconductive antenna with Drude-Lorentz Mode [24-25]. In Section 4-3, we

generate THz radiation using chirp controller of femtosecond optical pulses. In Section 4-4, we generate THz radiation using multi-peak femtosecond pulses and discuss the experiment results.

The Application of Pulse Shaping in THz Waveform Synthesis

The generation of coherent radiation across the electromagnetic spectrum has enabled the technologies that have a defining impact on life in the 21st century. However, a gap in technology exists in the terahertz (THz) frequency regime, between 100 GHz and 10 THz (wavelengths between 30 mm and 3 mm). Historically, it has been technically difficult to generate, manipulate, and detect radiation in this portion of the electromagnetic spectrum where electronics transitions to photonics. A desire to develop this wavelength regime is fueled by potentially important applications in remote sensing, communications, signal processing, materials characterization and control, biological and medical imaging, and non-destructive evaluation (NDE). Ultrafast laser technology has made significant contributions towards expanding photonics to the THz regime. The technique of terahertz time domain spectroscopy (THz-TDS) generates broadband, single cycle THz pulses of subpicosecond duration using resonant femtosecond (fs) optical excitation of biased semiconductor strip-lines or nonresonant optical rectification in electro-optic crystals. The coherent detection of the THz electric field is similarly achieved using fs optical gating pulses. Since THz-TDS is a coherent free-space opticallygated technique it has distinct advantages in comparison to conventional far-infrared (optical) detection techniques. The coherent

nature of THz-TDS yields a much greater brightness in comparison to thermal sources and optical-gating discriminates against thermal background leading to, in some cases, a signal-to-noise ratio (S/N) approaching 10^6 . Indeed, using an optoelectronic technique based on semiconductor strip-lines, a spatially and temporally coherent beam of THz radiation from 0.1 to 5 THz can be generated and detected with $S/N > 10^5$, while nonlinear optical methods based on optical rectification have generated 50 fs THz pulses with frequencies from 0.1 to .40 THz that are detected with $S/N = 1000:1$. Further, THz-TDS measures the electric field (i. e., amplitude and phase) of the THz pulse with high linearity. Fourier transformation of the measured THz field, after propagation through a sample (and a suitable reference) allows for the direct experimental determination of both the real and imaginary parts of the dielectric response (or equivalently, conductivity) as a function of frequency obviating the need for delicate Kramers-Kronig analysis. The THz pulses are derived from a coherent optical source, enabling synchronized optical excitation useful both for time-resolved spectroscopic studies and two-color schemes for communications, remote sensing, imaging, and signal processing. For many of the envisioned applications of THz technology, the ability to generate and manipulate the radiation in a variety of formats is required. For example, temporally shaped pulse trains will be needed for communications, signal processing and materials control, broadband pulses for remote sensing and materials characterization, and tunable narrow-band radiation for enhanced imaging. The design of the THz waveforms was performed via spectral shaping of the pump laser pulse in a phase-only pulse shaper. The desired optical intensity targets typically consisted of trains of pulses with variable pulse widths and pulse separations in the time domain.

4-1.Principles of Optically Excited and Detected THz Radiation and its Applications

A popular method to generate or detect THz radiation is using photoconductive (PC) antennas or electro-optic (EO) materials illuminated with fs laser pulses. Because we use antennas to yield THz, the principles of optically excited and detected THz radiation would be directed in the following sections.

4-1.1 Generation of THz Radiation Using PC Antennas

When a femtosecond (fs) laser excites a biased semiconductor with photon energies greater than its bandgap, electrons and holes are produced at the illumination point in the conduction and valence bands, respectively. An electromagnetic field radiating into free-space with the help of an antenna is produced by the fast changes of the density of photocarriers and their acceleration due to the applied dc bias (V_b). The production of ultrashort currents with a full-width half-maximum (FWHM) of 1ps or less strongly depends on the carrier lifetime in the semiconductor.

The carrier density behavior in time is given by

$$\frac{dn}{dt} = -n/\tau_t + G(t) \quad (4.1)$$

where n is the carrier density and $G(t) = n_0 \exp(t/\Delta t)^2$ is the generation rate of carriers due to laser pulse excitation, with t the laser pulse width and n_0 the generated carrier density at $t = 0$. The generated carriers are accelerated by the electric field bias with a velocity rate given by

$$\frac{dv_{e,h}}{dt} = -v_{e,h}/\tau_{rel} + (q_{e,h}E)/m_{eff,e,h} \quad (4.2)$$

where $v_{e,h}$ are the average velocity of the carrier, $q_{e,h}$ are the charge of the electron and

hole, τ_{rel} is the momentum relaxation time, and E is the local electric field, which is less than the applied bias E_b due to the screen effect of space charges. More precisely,

$$E = E_b - P/3\epsilon_r \quad (4.3)$$

where ϵ_r is the dielectric constant and P is the polarization induced by the separation of electrons and holes. The polarization depends on time according to the expression

$$dP/dt = -P/\tau_{rec} + J \quad (4.4)$$

where τ_{rec} is the recombination time between electrons and holes ($\tau_{rec} = 10$ ps for LT-GaAs) and $J = env_h + (-e)nv_e$ is the current density. The far-field radiation is given by

$$E_{THz} \propto \partial J / \partial t \propto ev \partial n / \partial t + en \partial v / \partial t, \quad (4.5)$$

where $v = v_e - v_h$. The transient electromagnetic field E_{THz} consists of two terms: the first term describes the carrier density charge effect while the second term describes the effect of charge acceleration due to the electric field bias.

4-1.2 Detection of THz Radiation Using PC Antennas

The electric field of a Gaussian beam on the detector as shown in Fig. 2.1 can be expressed as:

$$E(x, y) = E_0 \exp[-(x^2 + y^2)/w_l^2] \quad (4.8)$$

where w_l is spot size. The total resistance over the detector is:

$$R = \frac{\rho_M L_M + \rho_S L_S}{td} \approx \frac{\rho_S L_S}{td} \quad (4.9)$$

where L_M is the total length of the metal electrodes, L_S is the length of the switch area between the two electrode tips, ρ_M and ρ_S are their resistivities, respectively, and d is the width of the electrode and the gap area. The average resistivity ρ_S is much

larger than ρ_M owing to the low duty cycle of the driving laser (100 fs/10 ns = 10^{-5}).

The resistivity ρ_S depends on the photogenerated carrier density, which for homogeneous illumination of power P_{laser} scales as

$$\rho_S = \frac{L_S d}{\xi P_{laser}} \quad (4.10)$$

where ξ is a conversion factor between laser power and number of photogenerated carriers. The average field strength \overline{E} across the detector gives rise to a potential difference $U = \overline{E}(L_M + L_S)$, so the average current is

$$I = \frac{U}{R} = \frac{\overline{E}(L_M + L_S)}{L_S^2} t d \xi P_{laser} \quad (4.11)$$

The average electric field across the detector area is

$$\begin{aligned} \overline{E(L, d)} &= \frac{1}{Ld} \int_{-L/2}^{L/2} \int_{-d/2}^{d/2} E(x, y) dx dy \\ &= \frac{E_0 \pi w_1^2}{Ld} \text{Erf}\left(\frac{L}{2w_1}\right) \text{Erf}\left(\frac{d}{2w_1}\right) \end{aligned} \quad (4.22)$$

where Erf is the error function, and $L = L_M + L_S$. The peak strength of the electric field, E_0 , can be expressed in terms of the total power in the THz beam:

$$P_{THz} = \frac{1}{2} c \epsilon_0 \int_{-\infty}^{\infty} \int_{-\infty}^{\infty} E^2(x, y) dx dy = \frac{1}{2} \pi w_1^2 c \epsilon_0 E_0^2 \quad (4.13)$$

$$\Rightarrow E_0 = \frac{2}{w_1} \sqrt{\frac{P_{THz}}{\pi c \epsilon_0}} \quad (4.14)$$

By inserting Eq. (2.14) into the expression for the detector current, Eq. (4.11), we get

$$I(\nu) = \xi P_{laser} \sqrt{\frac{c P_{THz}}{\pi \epsilon_0}} \frac{2 R_L t}{L_S^2 d \omega_0 (n-1) \nu} \text{Erf}\left[\frac{L (n-1) \pi w_0}{2 c R_L} \nu\right] \text{Erf}\left[\frac{d (n-1) \pi w_0}{2 c R_L} \nu\right] \quad (4.15)$$

when focusing spot size $\lim_{\lambda \rightarrow 0} w_1(d_{focus}) = \frac{c}{\pi \nu \omega_0} \frac{R_L}{(n-1)}$.

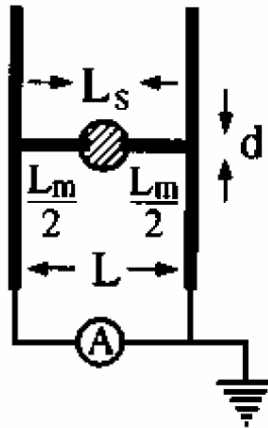


Fig. 4.1 Structure of antenna detector

4-1.3 Applications

THz technologies have made great progress for aiming at applications such as radio astronomy, remote-sensing, spectroscopy, optical properties of semiconductors and dielectrics, imaging of general substances, and biomedical imaging. It also can be applied to find specific spectroscopic fingerprints of biological matter in this region.

4-2.Simulation of THz Radiation with Drude-Lorentz

Model

In this section, we present detailed calculations of carrier dynamics and THz radiation on biased semiconductors with different theory Drude-Lorentz model [24-25]. When a biased semiconductor is pumped by a ultrafast laser pulse, the rapid change of the transport photocurrent gives rise to electromagnetic radiation. The change in photocurrent J ($J = env$, where e is the carrier charge, v the carrier speed, and n the carrier density), arises from two processes: the acceleration of photogenerated carrier under an electric field, $e n \partial v / \partial t$, and the rapid change of the carrier density via femtosecond laser pumping, $e v \partial n / \partial t$. Therefore, the electromagnetic radiation from a biased semiconductor can be divided into two parts according to its origin: one part is due to carrier acceleration, and the other part is due to the change in carrier density. Our calculations are based on the Drude-Lorentz theory of carrier transports in semiconductors. In the calculation model, we consider THz radiation from biased photoconductive antenna pumped by interaction between electrons and holes, trapping of carriers in mid-gap states, scattering of carriers, and dynamical space-charge effects. Our calculation results reveal that THz radiation due to ultrafast carrier density change is more prominent than THz radiation due to carrier acceleration. This result indicates that when the density of the moving carrier changes for any reason, for example, by laser pumping, trapping in defect levels, or recombination, the charged carrier will emit electromagnetic even in the absence of an electric field and consequently undergo no acceleration.

Drude-Lorentz is for a low-temperature-grown GaAs (LT-GaAs) photoconductor. This material has attracted great interest for ultrafast photonic applications because of

its short carrier lifetime, reasonably high mobility and high breakdown electric field. The carrier lifetime can be reduced to picoseconds or even sub-picoseconds in low-temperature-grown materials. For the calculations of carrier transport and THz radiation in a biased semiconductor, the one-dimensional Drude-Lorentz model is used. When a biased semiconductor is pumped by a laser pulse with photon energies greater than the band gap of the semiconductor, electrons and holes are created in the conduction band and valence band, respectively, In LT-GaAs, the carrier pumped by ultrashort laser pulse is trapped in the mid-gap states with the time constant of the carrier trapping time. The time dependence of the carrier density is given by Eq.4-3-1, where τ_c is the trapping time and $G(t)$ describes the generation of free carriers by the laser pulse:

$$\frac{dn_f}{dt} = -\frac{n_f}{\tau_c} + G(t) \quad \dots\dots\dots 4-3-1$$



The time dependence of the average velocity is in the Drude-Lorentz picture, given as

$$\frac{dv(t)}{dt} = -\frac{v}{\tau_s} + \frac{e}{m^*} E_{mol} \quad \dots\dots\dots 4-3-2$$

where τ_s is the momentum relaxation time, m^* is the effective mass, and E_{mol} is the electric field at the position of the carriers, given by

$$E_{mol} = E_{bias} - \frac{P_{sc}}{\eta\epsilon} \quad \dots\dots\dots 4-3-3$$

where P_{sc} is the space-charge polarization created by the carriers separating in the field. The geometrical factor h is equal to three for an isotropic dielectric material.

The time dependence of the space-charge polarization can be represented by

$$\frac{dP_{sc}}{dt} = -\frac{P_{sc}}{\tau_r} + n_f e v \dots\dots\dots 4-3-4$$

where τ_r is the recombination lifetime. In general, $t_s \ll t_c \ll \tau_r$, where typical values are t_s , 100 fs and t_c , τ_r ; 1 – 100 ps.

For the numerical calculations, we use the effective mass of the electrons and holes given by $m_e = 0.067m_0$ and $m_h = 0.37 m_0$, respectively. The momentum relaxation time is taken to be 30 fs for both, the electrons and holes. The carrier generation rate $G(t)$ is assumed to be a Gaussian-type function of time t , $n_0 \exp(-t^2/\Delta t^2)$, where n_0 represents the carrier generation density at $t = 0$ ps.

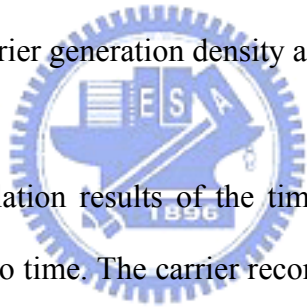


Fig.4-1 shows the calculation results of the time dependent photocurrents and their derivatives with respect to time. The carrier recombination time τ_r is taken as 10 ps. The other values of the carrier recombination time τ_r , longer than 10 ps, have little effect on the calculated THz waveform. The time-dependent photocurrents at carrier trapping times τ_c of 0.1, 0.5, 1.0, 2.0, and 5.0 ps are shown in **Fig. 4-1(a)**. Figure 1(b) depicts the time derivatives of the photocurrents shown in **Fig. 4-1(a)**. The waveform of THz radiation is similar to that of the time derivative of transient photocurrent. As shown in **Fig.4-1(b)**, the positive peak of THz radiation arises from the steep rising edge of the photocurrent, and the negative peak arises from the falling edge of the photocurrent. The negative peak is always smaller than the positive peak because of the finite lifetime of the carrier. As a result, the amplitude and spectral bandwidth of THz radiation are primarily determined by the rising edge of the photocurrent. From **Fig. 4-1(b)**, it is noted that the electromagnetic radiation is mostly limited to a time

scale of 2–3 ps, and the waveform does not change significantly with the change of the carrier trapping time, ζc . This cannot be explained by the assumption that a major portion of electromagnetic radiation is proportional to carrier acceleration. The excited carriers will be accelerated continuously as long as the local electric field and the carrier density are not zero. Hence, the waveform of the electromagnetic field proportional to the acceleration of the carrier will depend strongly on the carrier trapping times.

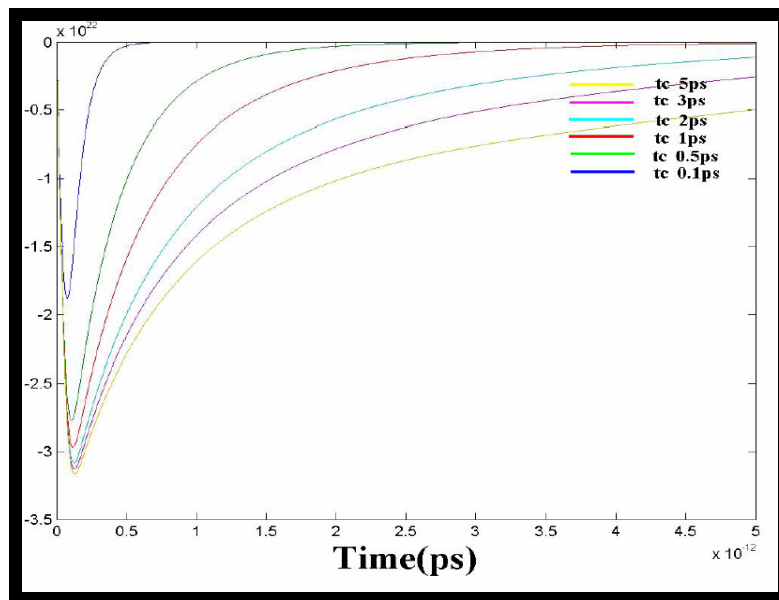


Fig.4-1. (a) Waveforms of photocurrents and **(b)** their time derivatives as a function of time at trapping times ζc of 0.1, 0.5, 1.0, 2.0, and 5.0 ps. The waveform of the THz pulse is similar to that of the time derivative of the photocurrent.

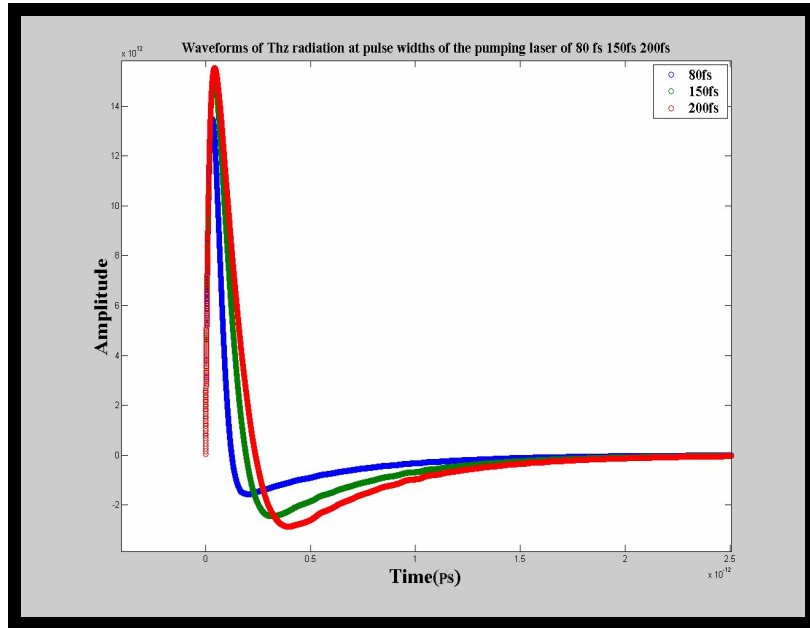


Fig.4-2 The waveforms of the THz pulse for laser pulse widths Δt of 80, 150, and 200 fs. As shown in Fig. 2 the THz pulse widens as the excitation laser pulse width increases. The spectral bandwidth of THz radiation also changes considerably as the width of the laser pulse changes.

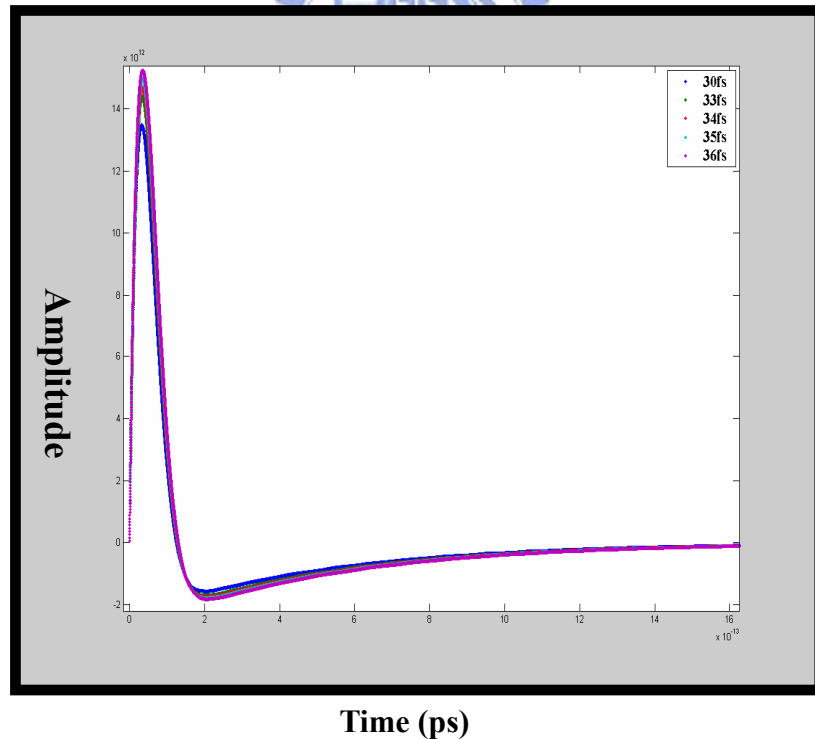


Fig.4-3 depicts the waveforms of the THz pulse for different relaxation time t_s of 30, 33, 34, 35, 36 fs. As shown in Fig. 3 the THz waveform does not change significantly with the change of the relaxation time t_s , but the amplitude is become large as the relaxation time increased.

4-3. Generation of THz Radiation Using Chirp Controller of Femtosecond Optical Pulses

The design of the THz waveforms was performed via spectral shaping of the pump laser pulse in a phase-only pulse shaper. If we produce different pulse width of femtosecond optical laser to generate THz radiation, we are expected to obtain the same results that we simulate in **Fig.4-2**. We use the synthesis of femtosecond optical pulses including adaptive pulse shaping with freezing phase scheme and synthesis of femtosecond optical pulses with Gerchberg-Saton algorithm to yield the pulse with different pulse width. **Fig 4-4** shows that the different pulse width which is broadened by negative or positive chirp made by SLM. The pulses are broadened by with positive and negative chirp and the relation between chirp value and pulse width shows in **Fig 4-5**. **Fig 4-6** shows the setup of terahertz time domain spectroscopy. We use different pulse width to generate the THz radiation and to compare the difference between the experimental results and the simulations. The positive chirp, 164070fs^2 and 82035fs^2 are made by pulse shaping system; bring about 900fs and 600fs laser pulse. The spectral bandwidth of THz radiation generated with transform-limited pulse is the broadest than 900fs and 600fs laser pulse. Base on the result of simulation, the THz pulse widens as the excitation laser pulse width increases, the slimly phenomenon in experiment showed in **fig4.7** is obtained.

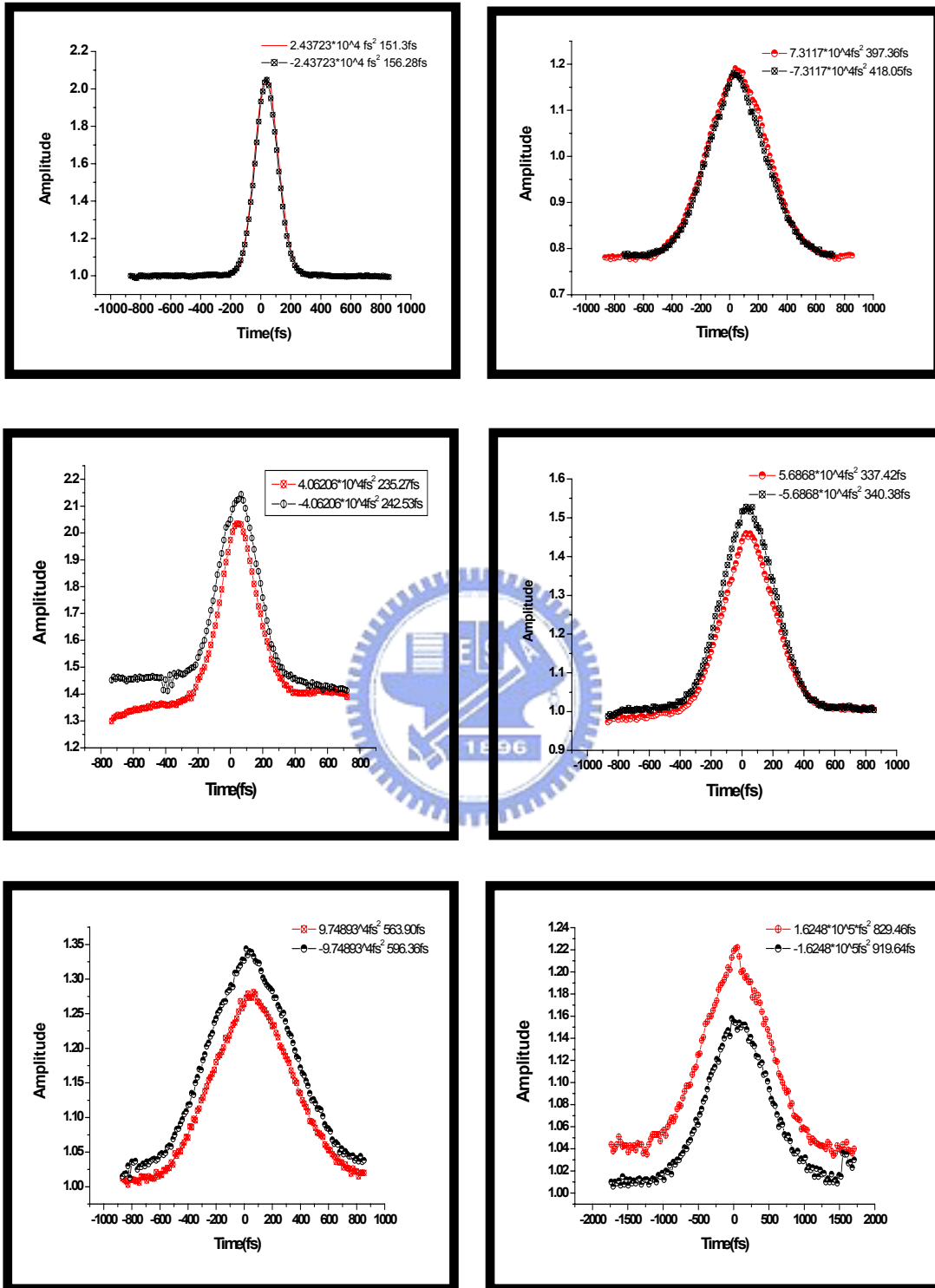


Fig 4-4 The different pulse width which is broadened by negative or positive chirp is made by SLM. Red line means the pulse broadened by positive chirp and break line means the negative chirp.

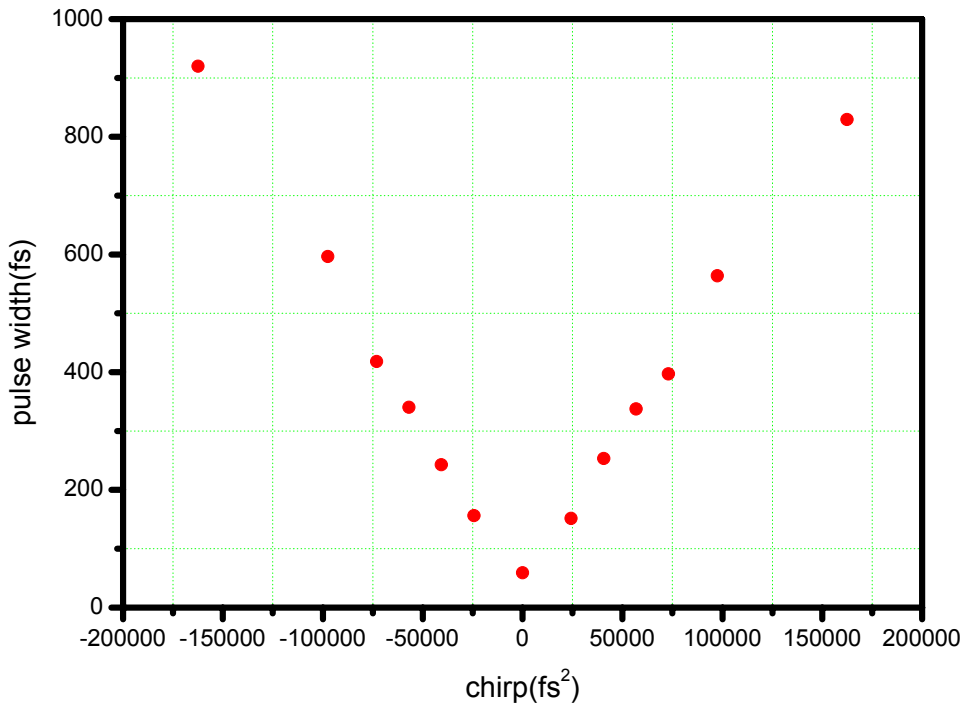


Fig 4-5 The relation between the chirp and pulse width.

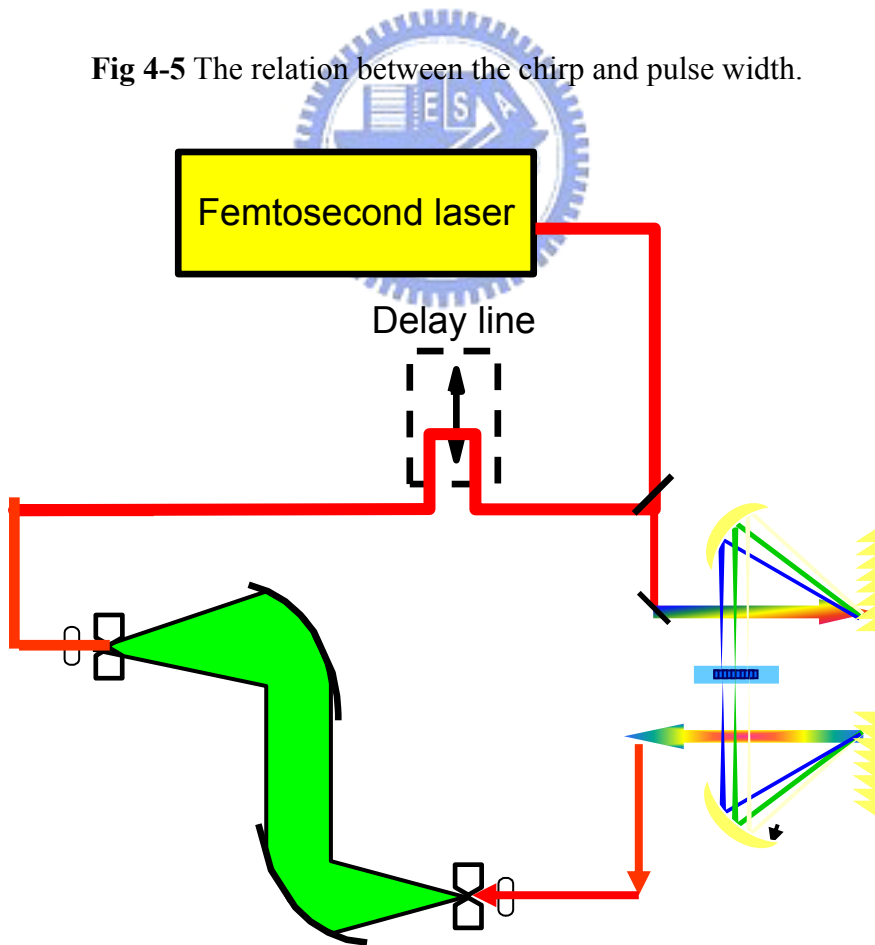


Fig 4-6 The setup of terahertz time domain spectroscopy and pulse shaping system

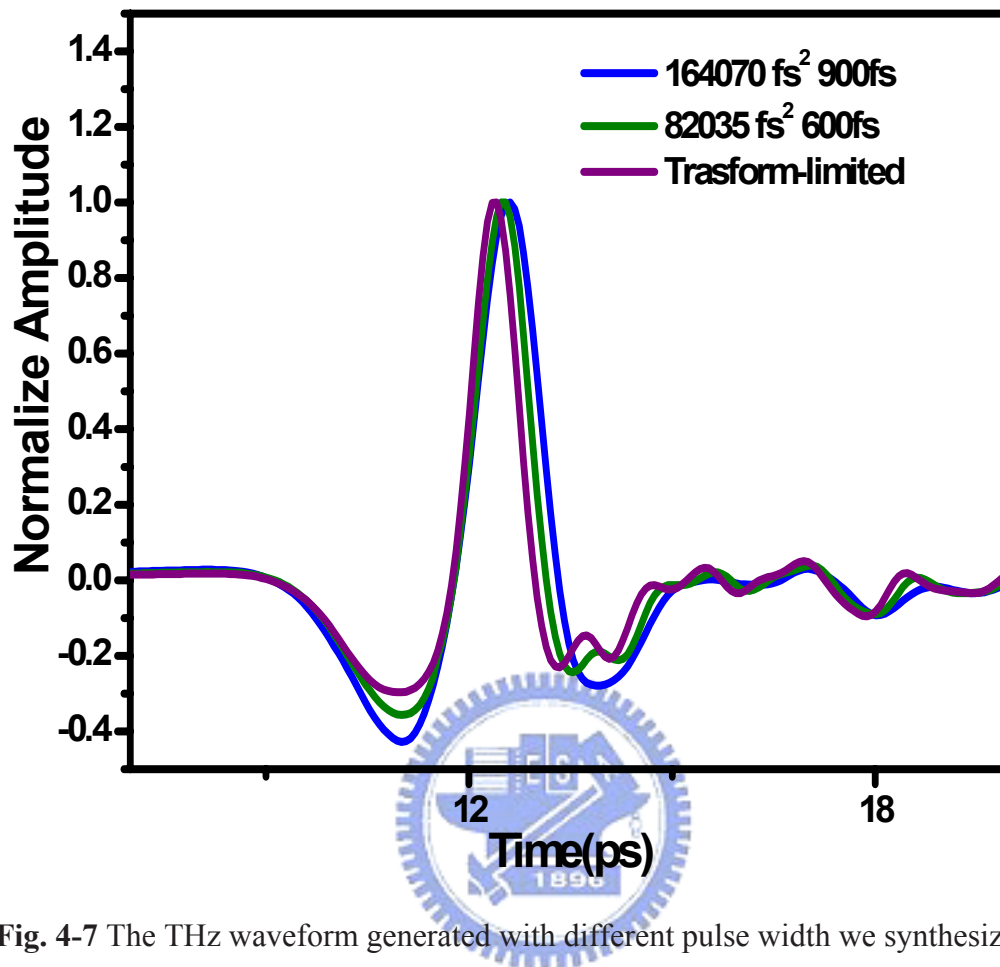


Fig. 4-7 The THz waveform generated with different pulse width we synthesize.

The THz pulse widens as the excitation laser pulse width increases, the slimily phenomenon in simulation showed in **fig4.2** is obtained. For blue curve and green curve, laser pulse width = 900fs and 600fs. Purple curve represent the THz radiation is yielded by transform-limited laser.

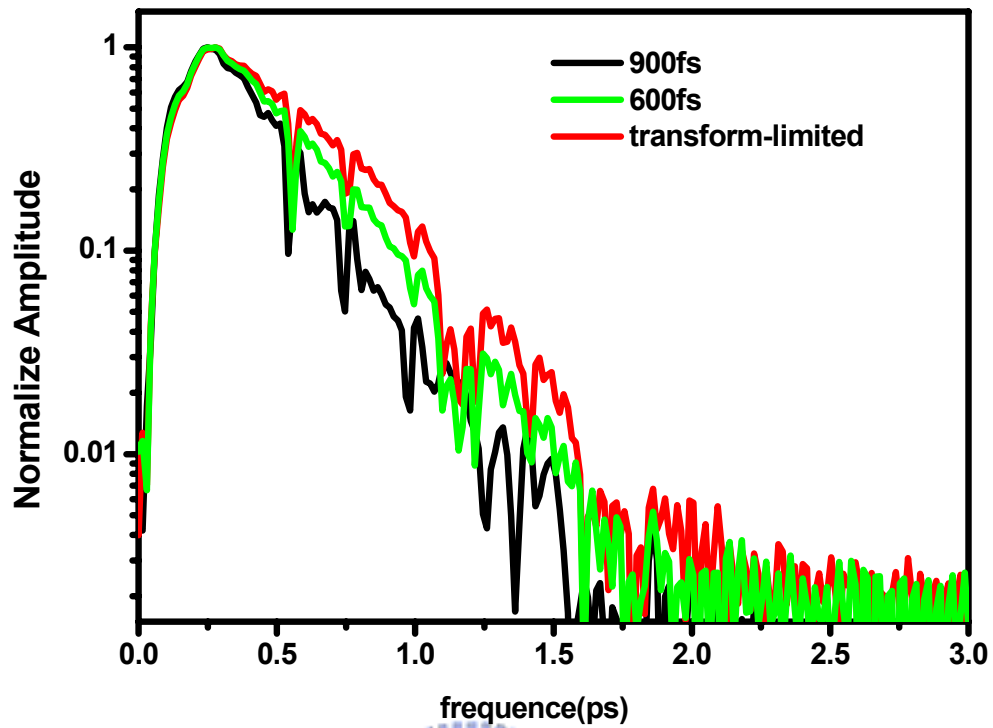


Fig. 4-8 The spectrum of THz radiation generated with different pulse width we synthesize. Base on the result of experiment, the spectrum of THz radiation widens as the excitation laser pulse width decreases. For block curve and green curve, laser pulse width = 900fs and 600fs. Red curve represent the THz radiation is yielded by transform-limited laser.

4-4. Generation of THz Radiation

Using Multi-Peak Femtosecond Pulses

The design of the THz waveforms is performed via pulse shaping of the pump laser pulse in a phase-only pulse shaper. The desired optical intensity targets typically consisted of trains of pulses with variable pulse widths and pulse separations in the time domain. The shapes of the optical pulses are accomplished in section 3-3. **Fig. 4-9** shows the experimental setup including terahertz time domain spectroscopy (THz-TDS) and pulse shaping system. The numbers of pulses in the train of optical pump pulses with the 1ps pulse separation generate THz radiation and the result of the synthesized THz pulse can be presented in **Fig. 4-10-(a)~(c)**. In **Fig. 4-11**, the increasing numbers of THz oscillations influence the distribution of THz spectrum and enhance the amplitude of the spectrum in certain frequency. The number of pulses in the train of optical pump pulses and their spacing can be used to narrow the resulting THz spectrum and to tune its central frequency. Because the optical pulse train, which has many nearly identical optical pulses with equal spacing between the neighboring pulses, was programmed in a temporal window of 2 ps, the numbers of optical pulse train with 1ps separations(\geq carrier lifetime of GaAs) is three. The width of the programmable temporal window is limited by the spatial separation of the spectral filters and the spectral resolution of the pulse shaper is 50GHz. If the spectral resolution of the pulse shaper is achieved to 100GHz, THz spectrum can be narrowed and enhance amplitude in central frequency by more pulse train. The better results of the experiment can be completed. **Fig.4-12** shows the THz radiation with the different number of pulse in the temporal domain.

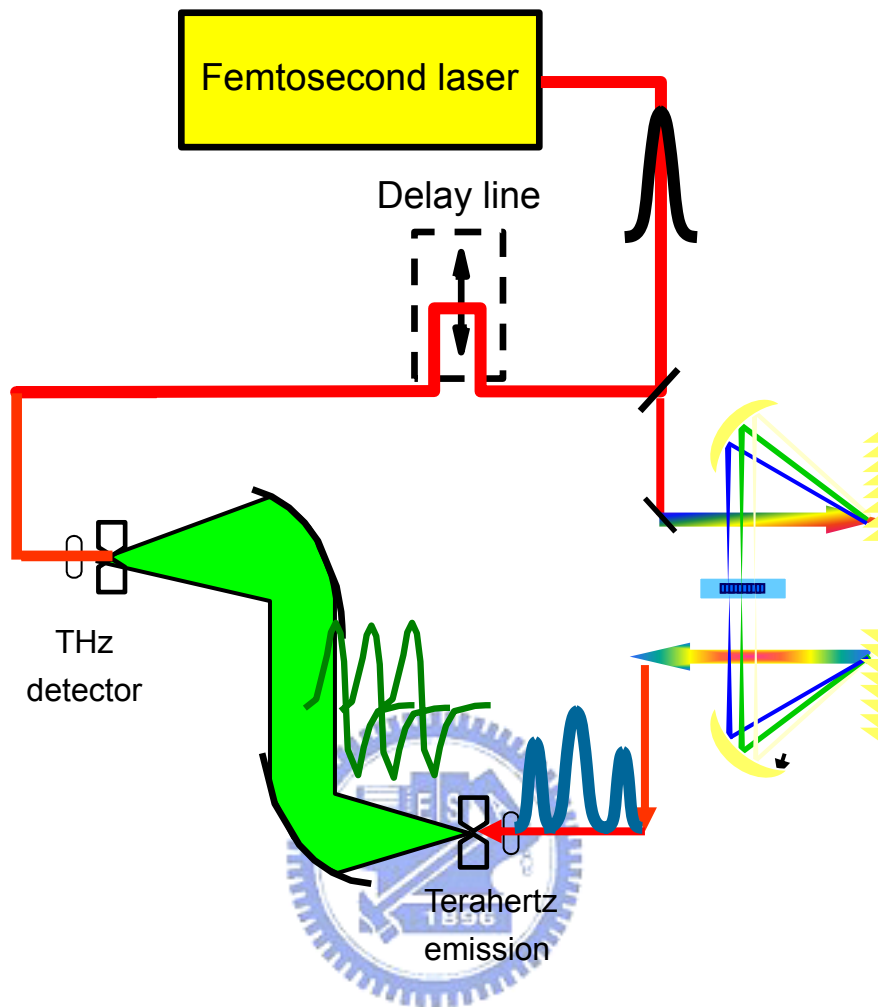
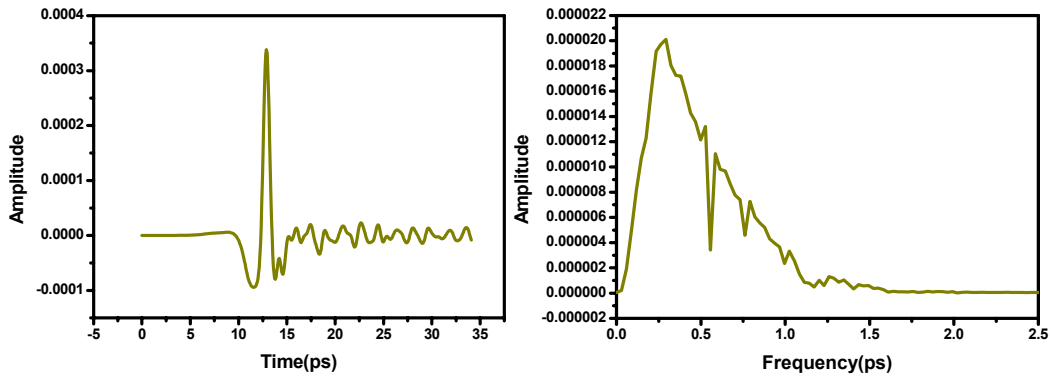
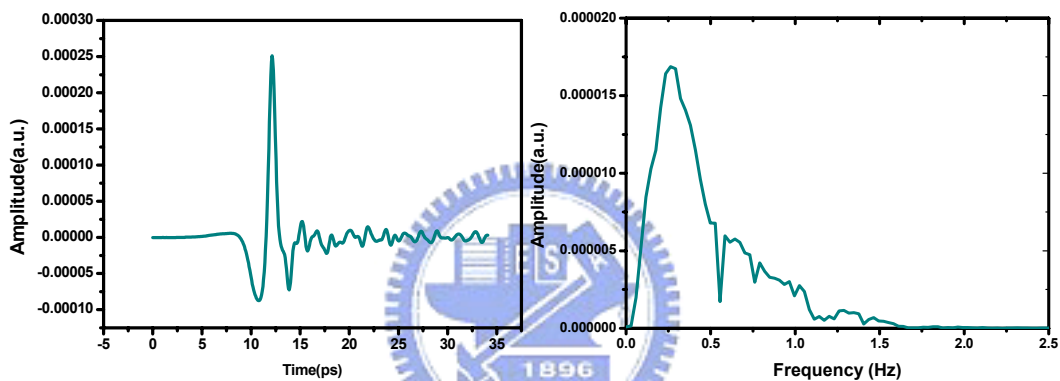


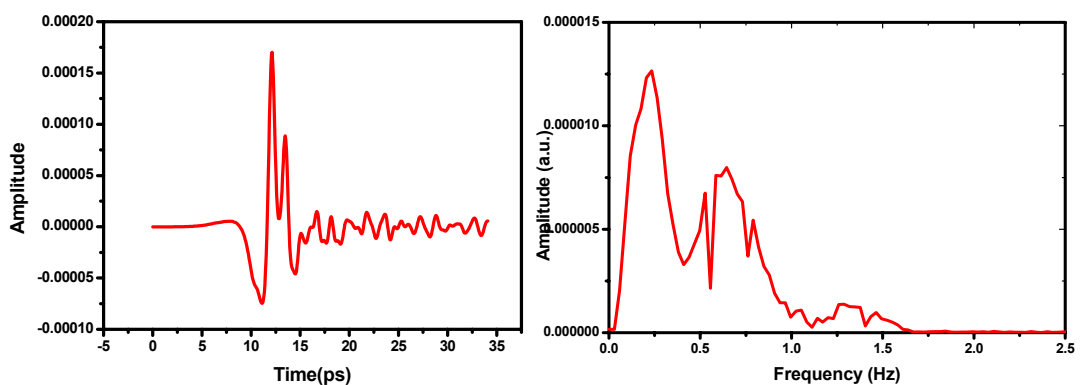
Fig. 4-9 The schematic diagram of experiment arrangement Pump laser pulses enter the apparatus and are spectrally dispersed in an optical pulse shaper which has a computer-controlled array of optical masks. The numbers of pulses in the train of optical pump pulses now generate the shaped terahertz pulses. The shape of the terahertz pulses are collected and guided by gold-coated parabolic mirrors. Femtosecond laser pulse as a probe beam with time delayed by motor stage and the shape THz pulse collinearly impinged on another dipole antenna with the GaAs substrate to detect THz radiation.



(a) Transform-limited laser pulse generates THz radiation. THz temporal shapes and the spectra of the THz pulses are shown in the left, and the right figure panel.



(b) Double laser pulse that duration between the pulses is smaller than 1ps generates THz radiation. THz temporal shapes and the spectra of the THz pulses are shown in the left, and the right figure panel.



(c) Double laser pulses generate THz radiation. THz temporal shapes and the spectra of the THz pulses are shown in the left, and the right figure panel.

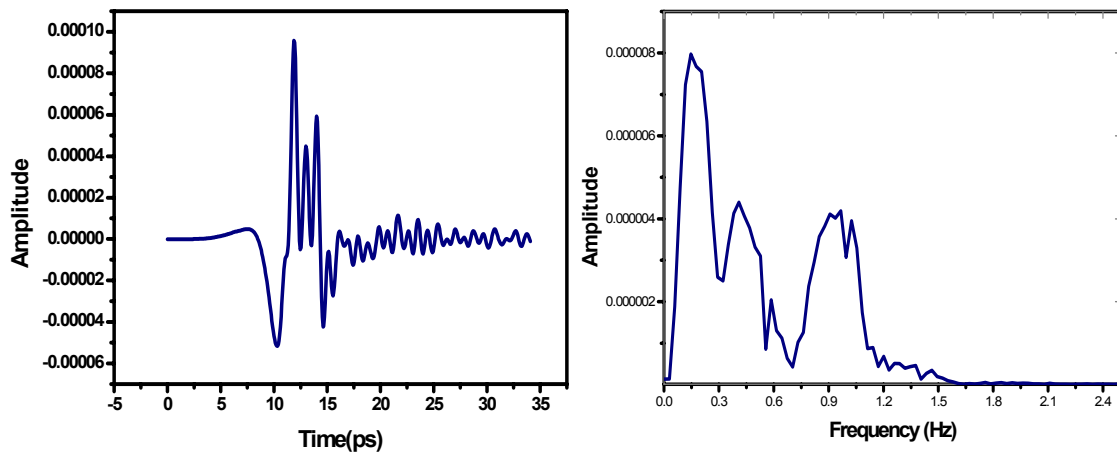


Fig.4-10. (c) Pulses trains of three pulses generate THz radiation. THz temporal shapes and the spectra of the THz pulses are shown in the left, and the right figure panel.

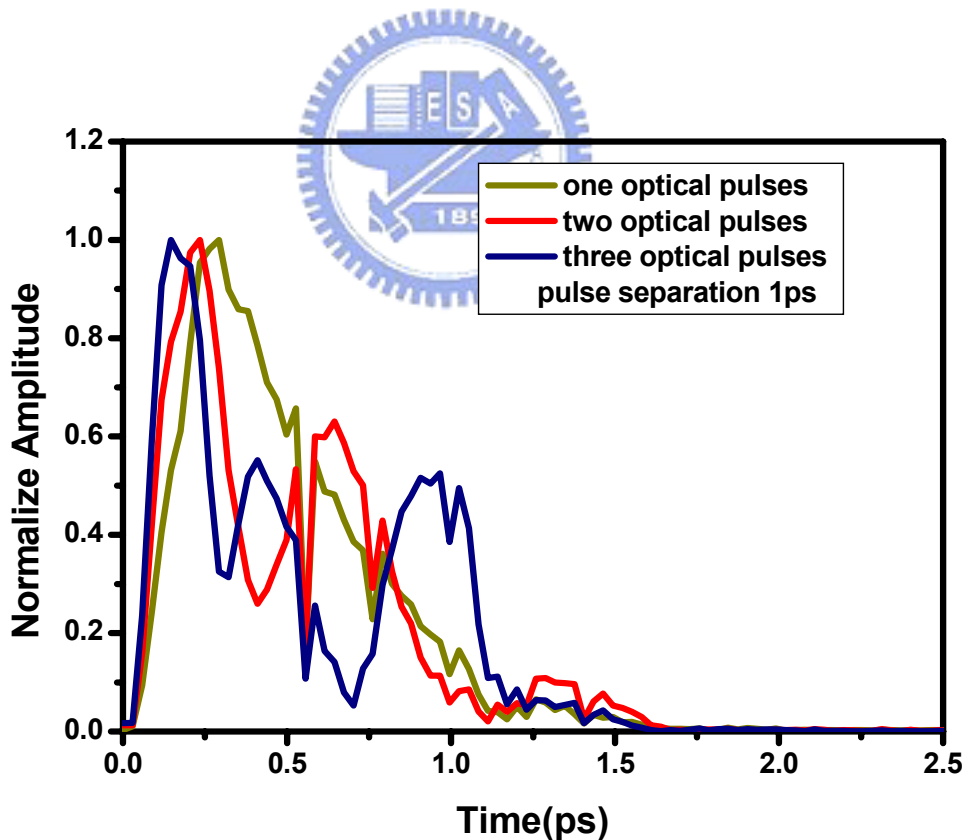


Fig. 4-11 The THz spectrum is generated by increasing numbers of optical pulses and the amplitude in spectrum is enhanced in some certain frequency.

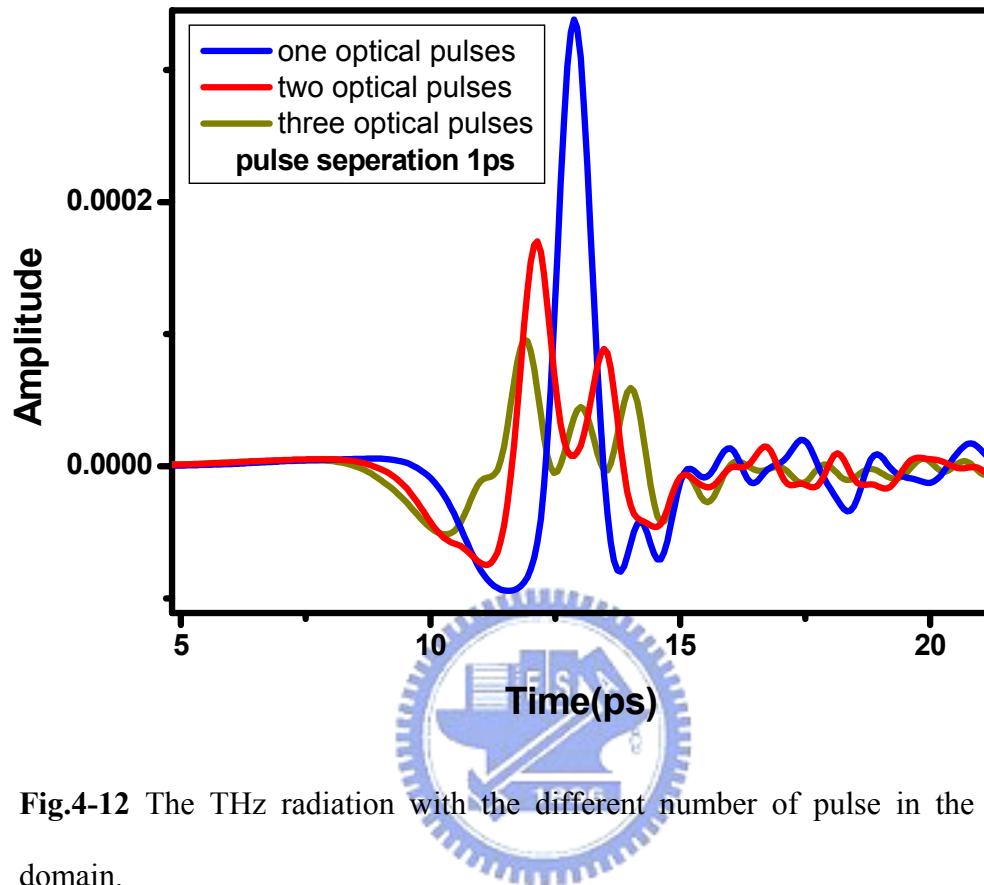


Fig.4-12 The THz radiation with the different number of pulse in the temporal domain.

Chapter5 Conclusion and Future Prospect

In this thesis, we demonstrate the optical synthesis technique for a desired ultrashort optical pulse with Gerchberg-Saxton algorithm (GS). By using an initial random phase pattern, GS achieves the target pulse faster as compared to that using an initial constant phase pattern. In order to design and shape the optical laser pulses, we have used computer-generated phase masks calculated using the Gerchberg-Saxton algorithm and implemented in a high precision spatial light modulation with 128 parallel phase masks. We use new freezing phase algorithm for complete-filed characterization of femtosecon ultrashort pulse with a phase-only pulse shaping apparatus to achieve transform-limited laser pulse. Based on the GS algorithm designing target pulse and freezing algorithm to achieve transform-limited, multi-pulse with different pulse duration, two pulses with dissimilar pulse duration and single pulse using unalike phase pattern to achieve different pulse width can be accomplished. From the experimental result in section 4-3~4-4, the application of the methodology on THz waveform synthesis based on radiation from ultrafast current surges in photoconductive antenna excited by shaped optical pulses is feasible. We have demonstrated a train and different bandwidth of THz pulses with pulse shaping system.

In addition to the controllability of terahertz radiation with more femtosecond pulse trains, we will show that optical pulse shaping can be used to avoid saturation of the terahertz field at highpeak power and increase generation efficiencies for terahertz radiations at selected, narrow-band frequencies in future work. . This freezing phase scheme had been employed for analyzing semiconductor saturable absorber Bragg

reflectors (SBR) and the detailed influence on phase distortion. We believe that this technique shall be useful for various future applications which require ultrashort pulse conversion, complete-field characterization and adaptive coherent control on the same setup.



Chapter6 References

1. A. Weiner, Review of Scientific Instruments, 71, 1929 (2000)
2. A. M. Weiner and J. P. Heritage, Rev. Phys. Appl. 22, 1619 (1987).
3. A. M. Weiner and A. M. Kanan, IEEE J. Sel. Top. Quantum Electron. 4, 317 (1998).
4. A. M. Weiner, in Trends in Optics and Photonics, edited by T. Asakura Springer, Berlin, (1999), pp. 233–246.
5. A. M. Weiner, Prog. Quantum Electron, 19, 161 (1995).
6. Andy Rundquist Anatoly Efimov* and David H. Reitze, J. Opt. Soc. Am. B 19, 10 (2002)
7. R. Mizoguchi and K. Onda, S. S. Kano, A. Wada Review of Scientific Instruments 74, 5 (2003)
8. A. Weiner, Review of Scientific Instruments, 71, 5 (2000)
9. A. M. Weiner, J. P. Heritage, and E. M. Kirschner, J. Opt. Soc. Am. B, 5, 8, (1988)
10. T. Baumert, T. Brixner, V. Seyfried, M. Strehle, G. Gerber Appl. Phys. B 65, 779–782 (1997)
11. Andrew M. Weiner, Fellow, IEEE, and Ayman M. Kan'an IEEE JOURNAL OF SELECTED TOPICS IN QUANTUM ELECTRONICS, 4, 2, (1998)
13. Anatoly Efimov, Mark D. Moores, Nicole M. Beach, Jeffrey L. Krause, and David H. Reitze OPTICS LETTERS, 23, 24 (1998)
14. D. E. Leaird and A. M. Weiner OPTICS LETTERS, 24, 12 (1999)
15. Andrew M. Weiner, Fellow, IEEE, and Ayman M. Kan'an IEEE JOURNAL OF SELECTED TOPICS IN QUANTUM ELECTRONICS, 4, 2, (1998)

16. U. Siegner and M. Haiml, J. Kunde and U. Keller OPTICS LETTERS, 27, 5 (2002)
17. E. Zeek, R. Bartels, M. M. Murnane, H. C. Kapteyn, and S. Backus G. Vdovin OPTICS LETTERS, 25, 8 (2002)
18. *Frequency-Resolved Optical Gating: The Measurement of Ultrashort Laser Pulses*, Rick Trebino, ed. (Kluwer Academic Publishers, Boston, 2002).
19. A. M. Weiner and D. E. Leaird OPTICS LETTERS, 15, 1(1996)
20. IEEE JOURNAL OF SELECTED TOPICS IN QUANTUM ELECTRONICS, 2, 3, (1996)
21. J. Ahn, A. V. Efimov, R. D. Averitt, and A. J. Taylor OPTICS EXPRESS 11, 20, 2486 (2003)
22. L. Xu, X.-C. Zhang, and D. H. Auston, Appl. Phys. Lett. 61, 1784-1786 (1992).
23. J. Y. Sohn, Y. H. Ahn, D. J. Park, E. Oh, and D. S. Kim, Appl. Phys. Lett. 81, 13 (2002).
24. Yongqian Liu, Sang-Gyu Park, and A. M. Weiner OPTICS LETTERS, 21, 21(1996)
25. Zhisheng PIAO, Masahiko TANI and Kiyomi SAKAI, Jpn. J. Appl, Phys, 39, 96-100, (2000).
27. P. Uhd Jepsen, R. H. Jacobsen, and S. R. Keiding J. Opt. Soc. Am. B., 13, 11 (1996)